The Astrophysical Journal, 892:105 (23pp), 2020 April 1 https://doi.org/10.3847/1538-4357/ab791e
© 2020. The American Astronomical Society. All rights reserved.

The Fourth Catalog of Active Galactic Nuclei Detected by the *Fermi* Large Area Telescope

M. Ajello[1], R. Angioni[2,3], M. Axelsson[4,5], J. Ballet[6], G. Barbiellini[7,8], D. Bastieri[9,10], J. Becerra Gonzalez[11], R. Bellazzini[12], E. Bissaldi[13,14], E. D. Bloom[15], R. Bonino[16,17], E. Bottacini[15,18], P. Bruel[19], S. Buson[20], F. Cafardo[21], R. A. Cameron[15], E. Cavazzuti[22], S. Chen[9,18], C. C. Cheung[23], S. Ciprini[3,2], D. Costantin[24], S. Cutini[25], F. D'Ammando[26], P. de la Torre Luque[13], R. de Menezes[17,21], F. de Palma[16], A. Desai[1], N. Di Lalla[15], L. Di Venere[13,14], A. Domínguez[27], F. Fana Dirirsa[28], E. C. Ferrara[29], J. Finke[23], A. Franckowiak[30], Y. Fukazawa[31], S. Funk[32], P. Fusco[13,14], F. Gargano[14], S. Garrappa[30], D. Gasparrini[2,3], N. Giglietto[13,14], F. Giordano[13,14], M. Giroletti[26], D. Green[33], I. A. Grenier[6], S. Guiriec[29,34], S. Harita[35], E. Hays[29], D. Horan[19], R. Itoh[36], G. Jóhannesson[37,38], M. Kovac'evic'[25], F. Krauss[39], M. Kreter[20,40], M. Kuss[12], S. Larsson[5,41,42], C. Leto[2], J. Li[30], I. Liodakis[15], F. Longo[7,8], F. Loparco[13,14], B. Lott[43], M. N. Lovellette[23], P. Lubrano[25], G. M. Madejski[15], S. Maldera[16], A. Manfreda[44], G. Martí-Devesa[45], F. Massaro[16,17,46], M. N. Mazziotta[14], I. Mereu[25,47], M. Meyer[32], G. Migliori[48,49], N. Mirabal[29,50], T. Mizuno[51], M. E. Monzani[15], A. Morselli[3], I. V. Moskalenko[15], M. Negro[50,52], R. Nemmen[21], E. Nuss[53], L. S. Ojha[29], R. Ojha[29], N. Omodei[15], M. Orienti[26], E. Orlando[15,54], J. F. Ormes[55], V. S. Paliya[30], Z. Pei[10], H. Peña-Herazo[16,17,46,56], M. Persic[7,57], M. Pesce-Rollins[12], L. Petrov[29], F. Piron[53], H. Poon[31], G. Principe[26], S. Rainò[13,14], R. Rando[9,18,58], B. Rani[29,59], M. Razzano[12,71], S. Razzaque[28], A. Reimer[15,45], O. Reimer[45], F. K. Schinzel[60,61], D. Serini[13], C. Sgrò[12], E. J. Siskind[62], G. Spandre[12], P. Spinelli[13,14], D. J. Suson[63], Y. Tachibana[35], D. J. Thompson[29], D. F. Torres[64,65], E. Torresi[66], E. Troja[29,67], J. Valverde[19], P. van Zyl[68,69,70], and M. Yassine[7,8]

[1] Department of Physics and Astronomy, Clemson University, Kinard Lab of Physics, Clemson, SC 29634-0978, USA
[2] Space Science Data Center—Agenzia Spaziale Italiana, Via del Politecnico, snc, I-00133, Roma, Italy; stefano.ciprini.asdc@gmail.com
[3] Istituto Nazionale di Fisica Nucleare, Sezione di Roma "Tor Vergata," I-00133 Roma, Italy; dario.gasparrini@ssdc.asi.it
[4] Department of Physics, Stockholm University, AlbaNova, SE-106 91 Stockholm, Sweden
[5] Department of Physics, KTH Royal Institute of Technology, AlbaNova, SE-106 91 Stockholm, Sweden
[6] AIM, CEA, CNRS, Université Paris-Saclay, Université Paris Diderot, Sorbonne Paris Cité, F-91191 Gif-sur-Yvette, France
[7] Istituto Nazionale di Fisica Nucleare, Sezione di Trieste, I-34127 Trieste, Italy
[8] Dipartimento di Fisica, Università di Trieste, I-34127 Trieste, Italy
[9] Istituto Nazionale di Fisica Nucleare, Sezione di Padova, I-35131 Padova, Italy
[10] Dipartimento di Fisica e Astronomia "G. Galilei," Università di Padova, I-35131 Padova, Italy
[11] Instituto de Astrofísica de Canarias, Observatorio del Teide, C/Via Lactea, s/n, E-38205, La Laguna, Tenerife, Spain
[12] Istituto Nazionale di Fisica Nucleare, Sezione di Pisa, I-56127 Pisa, Italy
[13] Dipartimento di Fisica "M. Merlin" dell'Università e del Politecnico di Bari, via Amendola 173, I-70126 Bari, Italy
[14] Istituto Nazionale di Fisica Nucleare, Sezione di Bari, I-70126 Bari, Italy
[15] W. W. Hansen Experimental Physics Laboratory, Kavli Institute for Particle Astrophysics and Cosmology, Department of Physics and SLAC National Accelerator Laboratory, Stanford University, Stanford, CA 94305, USA
[16] Istituto Nazionale di Fisica Nucleare, Sezione di Torino, I-10125 Torino, Italy
[17] Dipartimento di Fisica, Università degli Studi di Torino, I-10125 Torino, Italy
[18] Department of Physics and Astronomy, University of Padova, Vicolo Osservatorio 3, I-35122 Padova, Italy
[19] Laboratoire Leprince-Ringuet, École polytechnique, CNRS/IN2P3, F-91128 Palaiseau, France
[20] Institut für Theoretische Physik and Astrophysik, Universität Würzburg, D-97074 Würzburg, Germany
[21] Instituto de Astronomia, Geofísica e Ciências Atmosféricas, Universidade de São Paulo, Rua do Matão, 1226, São Paulo—SP 05508-090, Brazil
[22] Italian Space Agency, Via del Politecnico snc, I-00133 Roma, Italy
[23] Space Science Division, Naval Research Laboratory, Washington, DC 20375-5352, USA
[24] University of Padua, Department of Statistical Science, Via 8 Febbraio, 2, I-35122, Padova, Italy
[25] Istituto Nazionale di Fisica Nucleare, Sezione di Perugia, I-06123 Perugia, Italy
[26] INAF Istituto di Radioastronomia, I-40129 Bologna, Italy
[27] Grupo de Altas Energías, Universidad Complutense de Madrid, E-28040 Madrid, Spain
[28] Department of Physics, University of Johannesburg, P.O. Box 524, Auckland Park 2006, South Africa
[29] NASA Goddard Space Flight Center, Greenbelt, MD 20771, USA
[30] Deutsches Elektronen Synchrotron DESY, D-15738 Zeuthen, Germany
[31] Department of Physical Sciences, Hiroshima University, Higashi-Hiroshima, Hiroshima 739-8526, Japan
[32] Friedrich-Alexander Universität Erlangen-Nürnberg, Erlangen Centre for Astroparticle Physics, Erwin-Rommel-Str. 1, D-91058 Erlangen, Germany
[33] Max-Planck-Institut für Physik, D-80805 München, Germany
[34] The George Washington University, Department of Physics, 725 21st St, NW, Washington, DC 20052, USA
[35] Department of Physics, Tokyo Institute of Technology, Meguro City, Tokyo 152-8551, Japan
[36] Bisei Astronomical Observatory, 1723-70 Ookura, Bisei-cho, Ibara, Okayama 714-1411, Japan
[37] Science Institute, University of Iceland, IS-107 Reykjavik, Iceland
[38] Nordita, Royal Institute of Technology and Stockholm University, Roslagstullsbacken 23, SE-106 91 Stockholm, Sweden
[39] Department of Astronomy and Astrophysics, Pennsylvania State University, University Park, PA 16802, USA
[40] Centre for Space Research, North-West University, Potchefstroom Campus, Private Bag X6001, Potchefstroom 2520, South Africa
[41] The Oskar Klein Centre for Cosmoparticle Physics, AlbaNova, SE-106 91 Stockholm, Sweden
[42] School of Education, Health and Social Studies, Natural Science, Dalarna University, SE-791 88 Falun, Sweden
[43] Centre d'Études Nucléaires de Bordeaux Gradignan, Université de Bordeaux, IN2P3/CNRS, F-33175 Gradignan Cedex, France; lott@cenbg.in2p3.fr
[44] Università di Pisa and Istituto Nazionale di Fisica Nucleare, Sezione di Pisa I-56127 Pisa, Italy
[45] Institut für Astro- und Teilchenphysik, Leopold-Franzens-Universität Innsbruck, A-6020 Innsbruck, Austria
[46] Istituto Nazionale di Astrofisica-Osservatorio Astrofisico di Torino, via Osservatorio 20, I-10025 Pino Torinese, Italy
[47] Dipartimento di Fisica, Università degli Studi di Perugia, I-06123 Perugia, Italy

[48] Dipartimento di Astronomia, Università di Bologna, I-40127 Bologna, Italy
[49] Università di Bologna, I-40126 Bologna, Italy
[50] Department of Physics and Center for Space Sciences and Technology, University of Maryland Baltimore County, Baltimore, MD 21250, USA
[51] Hiroshima Astrophysical Science Center, Hiroshima University, Higashi-Hiroshima, Hiroshima 739-8526, Japan
[52] Center for Research and Exploration in Space Science and Technology (CRESST) and NASA Goddard Space Flight Center, Greenbelt, MD 20771, USA
[53] Laboratoire Univers et Particules de Montpellier, Université Montpellier, CNRS/IN2P3, F-34095 Montpellier, France
[54] Istituto Nazionale di Fisica Nucleare, Sezione di Trieste, and Università di Trieste, I-34127 Trieste, Italy
[55] Department of Physics and Astronomy, University of Denver, Denver, CO 80208, USA
[56] Instituto Nacional de Astrofísica, Óptica y Electrónica, Tonantzintla, Puebla 72840, Mexico; harold.penah@gmail.com
[57] Osservatorio Astronomico di Trieste, Istituto Nazionale di Astrofisica, I-34143 Trieste, Italy
[58] Center for Space Studies and Activities "G. Colombo," University of Padova, Via Venezia 15, I-35131 Padova, Italy
[59] Korea Astronomy and Space Science Institute, 776 Daedeokdae-ro, Yuseong-gu, Daejeon 305-348, Republic of Korea
[60] National Radio Astronomy Observatory, 1003 Lopezville Road, Socorro, NM 87801, USA
[61] University of New Mexico, MSC07 4220, Albuquerque, NM 87131, USA
[62] NYCB Real-Time Computing Inc., Lattingtown, NY 11560-1025, USA
[63] Purdue University Northwest, Hammond, IN 46323, USA
[64] Institute of Space Sciences (CSICIEEC), Campus UAB, Carrer de Magrans s/n, E-08193 Barcelona, Spain
[65] Institució Catalana de Recerca i Estudis Avançats (ICREA), E-08010 Barcelona, Spain
[66] INAF-Istituto di Astrofisica Spaziale e Fisica Cosmica Bologna, via P. Gobetti 101, I-40129 Bologna, Italy
[67] Department of Astronomy, University of Maryland, College Park, MD 20742, USA
[68] Hartebeesthoek Radio Astronomy Observatory, P.O. Box 443, Krugersdorp 1740, South Africa
[69] School of Physics, University of the Witwatersrand, Private Bag 3, WITS-2050, Johannesburg, South Africa
[70] Square Kilometre Array South Africa, Pinelands, 7405, South Africa
Received 2020 January 9; revised 2020 February 15; accepted 2020 February 17; published 2020 April 2

Abstract

The fourth catalog of active galactic nuclei (AGNs) detected by the *Fermi Gamma-ray Space Telescope* Large Area Telescope (4LAC) between 2008 August 4 and 2016 August 2 contains 2863 objects located at high Galactic latitudes ($|b| > 10^{\circ}$). It includes 85% more sources than the previous 3LAC catalog based on 4 yr of data. AGNs represent at least 79% of the high-latitude sources in the fourth *Fermi*-Large Area Telescope Source Catalog (4FGL), which covers the energy range from 50 MeV to 1 TeV. In addition, 344 gamma-ray AGNs are found at low Galactic latitudes. Most of the 4LAC AGNs are blazars (98%), while the remainder are other types of AGNs. The blazar population consists of 24% Flat Spectrum Radio Quasars (FSRQs), 38% BL Lac-type objects, and 38% blazar candidates of unknown types (BCUs). On average, FSRQs display softer spectra and stronger variability in the gamma-ray band than BL Lacs do, confirming previous findings. All AGNs detected by ground-based atmospheric Cerenkov telescopes are also found in the 4LAC.

Unified Astronomy Thesaurus concepts: Active galactic nuclei (16); Blazars (164); Gamma-ray sources (633); Relativistic jets (1390); Quasars (1319); BL Lacertae objects (158)

Supporting material: machine-readable tables

1. Introduction

Thanks to its broad energy range, excellent sensitivity, and all-sky monitoring capabilities, the *Fermi Gamma-ray Space Telescope* Large Area Telescope (LAT) has revolutionized our view of the gamma-ray sky. The fourth *Fermi*-LAT source catalog (4FGL, The Fermi-LAT collaboration 2020), based on the first 8 yr of data from the mission, contains 5064 sources in the energy range 50 MeV to 1 TeV.

The fourth catalog of active galactic nuclei (AGNs) detected by the LAT (4LAC), presented here, is derived from the 4FGL catalog. At high Galactic latitudes, AGNs represent by far the dominant class of gamma-ray sources in the 4FGL. The vast majority of these AGNs are of the blazar type, which are characterized by having relativistic jets closely aligned with our line of sight. The two main classes of blazars are Flat Spectrum Radio Quasars (FSRQs) and BL Lac-type objects (BL Lacs), distinguished according to the strength of their optical emission lines. FSRQs have strong, broad emission lines, while BL Lacs have weak, narrow, or no such lines. In addition to the improvements of the 4FGL relative to previous gamma-ray catalogs, the 4LAC has benefited from updated methods of associating gamma-ray AGNs with those known at other wavelengths. The 4LAC supersedes the third catalog of AGNs detected by the LAT (3LAC; Ackermann et al. 2015), which was based on 4 yr of data.

Gamma-ray AGN catalogs constitute unique resources for a broad range of astrophysics research. Recent applications include: population studies probing the BL Lac-FSRQ dichotomy (e.g., Ghisellini et al. 2017; Nalewajko & Gupta 2017); works on individual sources investigating the connections between gamma-ray loudness and brightness/polarization at other observational bands (e.g., Angelakis et al. 2016; Lico et al. 2017; Massaro et al. 2017; Fan & Wu 2018; Zargaryan et al. 2018); timing correlations between activity in the gamma-ray band and other wavelengths (e.g., Fuhrmann et al. 2016; Itoh et al. 2016); and tests of the possible link between gamma-ray AGNs and sources of ultra high-energy cosmic rays (e.g., Kagaya et al. 2017) or high-energy neutrinos (e.g., Padovani et al. 2016; Aartsen et al. 2017; Garrappa et al. 2019). These catalogs also enable probes of the extragalactic background light (EBL; e.g., Abdollahi et al. 2018) and the intergalactic magnetic field (e.g., Ackermann et al. 2018; Broderick et al. 2018), along with a measurement of the AGN contribution to the extragalactic diffuse gamma-ray background (e.g., Fornasa et al. 2016; Di Mauro et al. 2018).

The paper is organized as follows. Section 2 briefly describes the observations by the LAT and the analysis employed to

[71] Funded by contract FIRB-2012-RBFR12PM1F from the Italian Ministry of Education, University and Research (MIUR).

produce the eight-year catalog. In Section 3, we present the methods for associating gamma-ray sources with AGN counterparts and the different schemes for classifying them. Section 4 describes the contents of the 4LAC fits table and gives the statistics of the blazar and nonblazar populations. This section also includes a brief presentation of low-latitude ($|b| < 10°$) AGNs, which do not formally belong to the 4LAC. Some of the basic properties of the catalog sources are given in S5, along with a discussion of the overlap with the AGNs detected at very high energies (VHE; energies above 100 GeV) by atmospheric Cerenkov telescopes. Section 6 summarizes our findings.

In the following, we use a ΛCDM cosmology with values from the *Planck* results (Planck Collaboration et al. 2014); in particular, we use $h = 0.67$, $\Omega_m = 0.32$, and $\Omega_\Lambda = 0.68$, where the Hubble constant $H_0 = 100h$ km s^{-1} Mpc^{-1}.

2. Observations with the Large Area Telescope—Analysis Procedures

The 4LAC analysis was performed in the context of the 4FGL catalog, which is briefly summarized here. We refer the reader to the parent paper describing the 4FGL catalog for details (The Fermi-LAT collaboration 2020). The data were collected over the first 8 yr of the mission, from 2008 August 4 (MJD 54682) to 2016 August 2 (MJD 57602). The reprocessed P8R3_SOURCE_V2 event class (Bruel et al. 2018) data were used, with photon energies between 50 MeV and 1 TeV, broadening the energy interval with respect to the 100 MeV–300 GeV range of 3FGL (Acero et al. 2015). The increase in acceptance relative to the P7REP class used in 3FGL is 20% at high energies, accompanied by a better point-spread function (PSF). These improvements are beneficial to the source detection and localization, and hence to the counterpart association. A dedicated diffuse emission model was developed for analyses using the new event class. Weights penalizing photons with low energies and/or having directions close to the Galactic plane were introduced in the 4FGL likelihood to better account for systematic uncertainties. More details are available in Table 2 of the 4FGL paper. Different spectral models (power-law, log-parabola, power-law with superexponential cutoff) were tested, and the results are systematically reported in 4FGL. Sources with a maximum likelihood Test Statistic (TS) greater than 25 were retained in 4FGL, corresponding to a significance just over 4σ evaluated for the χ^2 distribution with four degrees of freedom. Variability was assessed via both 1 yr and 2 month light curves.

3. Source Association and Classification

The associations of 4FGL gamma-ray sources are based on positional coincidence with potential counterparts that display AGN-type spectral characteristics in the radio, infrared, optical, or X-ray bands. A conservative policy adopted early in the mission by the *Fermi*-LAT Collaboration is that firm identification is only claimed when correlated variability with a counterpart detected at lower energy has been reported. So far, only 78 AGNs have met this condition (see Table 7 of 4FGL). For the other sources, we use statistical approaches for finding associations between LAT sources and AGNs. The two approaches used here, the Bayesian method and the likelihood-ratio method, have been extensively described in previous catalogs (Abdo et al. 2010b; Ackermann et al. 2011, 2015) and are briefly summarized below.

Table 1
Catalogs Used for the Bayesian Association Method

Name	Objects[a]	References
BZCAT (Blazars)	3561	Massaro et al. (2015)
BL Lac	1371	Véron-Cetty & Véron (2010)
AGN	10066	Véron-Cetty & Véron (2010)
QSO	129,853	Véron-Cetty & Véron (2010)
Seyfert galaxies	27651	Véron-Cetty & Véron (2010)
Narrow-line Seyfert galaxies	18	Berton et al. (2015)
Narrow-line Seyfert galaxies	556	Rakshit et al. (2017)
FRICAT (radio galaxies)	233	Capetti et al. (2017a)
FRIICAT (radio galaxies)	123	Capetti et al. (2017b)
Giant Radio Source	349	Kuźmicz et al. (2018)
2WHSP	1691	Chang et al. (2017)
WISE blazar catalog	12319	D'Abrusco et al. (2014)
Radio Fundamental Catalog (2019a)	15740	http://astrogeo.org/rfc
CGRaBS	1625	Healey et al. (2008)
CRATES	11499	Healey et al. (2007)
ATCA 20 GHz southern sky survey	5890	Murphy et al. (2010)

Note.
[a] Number of objects in the catalog.

3.1. Source Association

3.1.1. The Bayesian Association Method

The Bayesian method was adapted for the *Fermi*-LAT catalogs following the work of Mattox et al. (1997) developed for the Energetic Gamma Ray Experiment Telescope (EGRET) on the *Compton Gamma Ray Observatory*. This method is described in Abdo et al. (2010b) and implemented with the *gtsrcid* tool.[72] The angular distance between a LAT source and a candidate counterpart corresponds to the position uncertainty in the case of a real association, while it is driven by the counterpart density in the case of a false (random) association. The prior distribution is fully characterized by a single number, which is the *a priori* probability that a given source of a catalog is the true counterpart of a gamma-ray source. This probability (referred to as the prior in the following) is assumed to be constant for a given catalog and is calibrated via Monte Carlo simulations so that the number of false associations, $N_{\rm false}$, is equal to the sum of the association-probability complements. For a given counterpart catalog, the prior is found to be close to $N_{\rm assoc}/N_{\rm tot}$, where $N_{\rm assoc}$ is the number of associations from this catalog and $N_{\rm tot}$ is the number of catalog sources. A uniform threshold of 0.80 is applied to the posterior probability for the association to be retained.

The list of catalogs used for the AGN associations with 4FGL sources is given in Table 1. With respect to 3LAC (Ackermann et al. 2015), updates of counterpart catalogs, e.g., BZCAT (Massaro et al. 2015), have been used when available. An important addition to the set of catalogs is the Radio

[72] https://fermi.gsfc.nasa.gov/ssc/data/analysis/scitools/overview.html

Fundamental Catalog[73] (RFC; Petrov et al. 2019), with 2720 associations with 4FGL sources (representing 85% of all AGNs). The high efficiency of association with VLBI catalogs that are sensitive to parsec-scale emission at 4–8 GHz is attributed to two factors: (1) the fact that γ-ray emission and parsec scale radio emission which originate from contemporary AGN activity are related, (2) the scarcity of radio sources with parsec scale emission at 4–8 GHz. The RFC includes many new entries that came from dedicated follow-up observations (Petrov et al. 2013; Schinzel et al. 2015, 2017) of unassociated gamma-ray sources, triggered by the publication of previous *Fermi*-LAT catalogs. Applying the Bayesian method to the whole catalog and retaining associations with $P \geqslant 0.80$, the association probability attached to the recent additions (181 sources) are reported as NULL to distinguish them for the others.

3.1.2. The Likelihood Ratio Association Method

The Likelihood Ratio (LR; e.g., de Ruiter et al. 1977; Cash 1979; Prestage & Peacock 1983; Sutherland & Saunders 1992; Lonsdale et al. 1998; Masci et al. 2001; Ackermann et al. 2011) method developed in the *Fermi*-LAT context makes use of large, relatively uniform surveys in the radio and in X-ray bands. These surveys enable us to search for possible counterparts among the faint radio and X-ray sources. The LR method is similar in nature to the Bayesian method, but the false association rate is computed from the density of objects brighter than the considered candidate, assessed from the survey log N–log S distribution. The method for computing the probability that a candidate is the "true" counterpart (called the reliability in this context) is described in detail in Section 3.2 of the 3LAC paper (Ackermann et al. 2015). A source is considered as a high-confidence counterpart of a given gamma-ray source if its reliability is greater than 0.80 for at least one survey.

For the LR approach, we analyzed the NRAO VLA Sky Survey (NVSS; Condon et al. 1998), the Sydney University Molonglo Sky Survey (SUMSS; Mauch et al. 2003), the Australia Telescope 20 GHz radio source catalog (Murphy et al. 2010), and the *ROSAT* All Sky Survey (RASS) Bright and Faint Source Catalogs (Voges et al. 1999, 2000). We also explored the second RASS catalog (Boller et al. 2016), but this attempt did not lead to further associations.

3.2. Association Results

The threshold adopted for the association probability is 0.80 in either method. This value represents a compromise between association efficiency and purity. The fraction of sources associated by both methods is 73% (2082/2863), with 684 and 97 sources being solely associated with the Bayesian and LR methods, respectively. The overall false-positive rate is 1.6%, where $N_{\rm false}$ is calculated as described in Section 3.1.1. The estimated number of false positives among the 1353 sources not previously reported in 3LAC is 35.6.

As in previous LAT AGN catalogs, we define a Clean Sample as those 4LAC sources that did not have any cautionary analysis flags, as described in Section 3.7.3 of the 4FGL paper (The Fermi-LAT collaboration 2020). The most frequent flags are flag 5 (source close to a brighter neighbor), flag 3 (large flux variation when changing diffuse emission model), and flag 2 (large position shift when changing diffuse emission model). Table 2 compares the performance of the two methods in terms of total number of associations $N_{\rm assoc}$, estimated number of false associations $N_{\rm false}$, and number of sources associated solely via a given method, N_S, for the full and Clean samples.

3.3. Source Classification

The classification of a source as an AGN primarily relies on its optical spectrum. Other characteristics, like the radio loudness, the presence of a flat/steep radio spectrum between 1.4 and 5 GHz, the broadband emission, the core compactness or the level of radio extended emission, the detection of variability, and the degree of polarization observed in different bands are used as ancillary information. If available, earlier classifications reported in the literature have been checked.

3.3.1. Optical Classification

The different resources used in the 4LAC for the optical classification are, in decreasing order of precedence:

1. Optical spectra from recent intensive follow-up programs (e.g., Shaw et al. 2013a, 2013b; Massaro et al. 2014, 2015a, 2015b, 2015c; Paggi et al. 2014; Landoni et al. 2015; Ricci et al. 2015; Álvarez Crespo et al. 2016a, 2016b, 2016c; Chiaro et al. 2016; Paiano et al. 2017a, 2017b, 2017c, 2019; Peña-Herazo et al. 2017; Landoni et al. 2018; Marchesi et al. 2018; de Menezes et al. 2019; Marchesini et al. 2019); these data are especially valuable for blazar candidates of previous LAT AGN catalogs that had never been observed.
2. The optical classification published in the BZCAT list, which is a compilation of sources classified as blazars (Massaro et al. 2015).
3. Spectra available in the literature or from online databases, e.g., the Sloan Digital Sky Survey (SDSS; Ahn et al. 2012; Massaro et al. 2014), 6dF Galaxy Survey (Jones et al. 2009), when more recent than the latest version of BZCAT (Massaro et al. 2015). The latter information was used only if the spectrum was published.

The relevant references are reported in the electronic table of the catalog. We did not use the blazar classes from the Simbad database,[74] since some of them correspond to predictions based on the *Wide-field Infrared Survey Explorer* (*WISE*)-strip approach (D'Abrusco et al. 2014) and were not obtained from spectral observations.

In the 4LAC, we classify the AGN-like gamma-ray detected objects adopting the following terminology:

1. Confirmed classifications:
   (a) FSRQ, BL Lac, radio galaxy, steep-spectrum radio quasar (SSRQ), compact steep spectrum radio source (CSS), Seyfert galaxy, and Narrow-line Seyfert 1 galaxy (NLSy1)—these are sources with a well-established classification in the literature and/or an optical spectrum with clear evidence for or lack of emission lines.
2. Tentative classifications:
   (a) BCU, blazar candidates of uncertain type: these are considered candidate blazars because the association

[73] Available at http://astrogeo.org/rfc.

[74] http://simbad.u-strasbg.fr/simbad/

Table 2
Comparison of Association Methods in Terms of Total Number of Associations, $N_{\rm assoc}$, Estimated Number of False Associations, $N_{\rm false}$, and Number of Sources Associated Only via a Given Method, $N_{\rm S}$

Sample	All Methods		Bayesian Method			LR Method		
	$N_{\rm assoc}$	$N_{\rm false}$	$N_{\rm assoc}$	$N_{\rm false}$	$N_{\rm S}$	$N_{\rm assoc}$	$N_{\rm false}$	$N_{\rm S}$
Full Sample	2863	44.4	2766	34.8	684	2179	143.1	97
Clean Sample	2614	36.5	2529	27.9	596	2018	130.9	85

methods (see Sections 3.1.1 and 3.1.2) select a candidate counterpart that satisfies at least one of the following conditions:

i. a BZU object (blazars of uncertain/transitional type) in the BZCAT list;
ii. a source with multiwavelength data in one or more of the *WISE*, AT20G, RFC (Petrov et al. 2019), CRATES (Healey et al. 2007), PMN-CA (Griffith & Wright 1993), CRATES-Gaps (Healey et al. 2009), or CLASS (Caccianiga et al. 2002) lists that indicates a flat radio spectrum and shows a typical two-humped, blazar-like spectral energy distribution (SED);
iii. a source included in radio and X-ray catalogs not listed above and for which we found a typical two-humped, blazar-like SED (see Böttcher 2007).

The scheme followed in 3LAC whereby BCUs were further divided in three subclasses according to the quality or availability of their optical spectra has not been reconducted in 4LAC. The large number of new BCU sources would have made this task excessively manpower-intensive.

(b) AGN—for these candidate counterparts, the existing data do not allow an unambiguous determination of the AGN type and do not meet any of the criteria to be classified as BCU. Their SEDs display properties typical of radio-loud compact core objects, but the literature information is either incomplete or conflicting for different epochs or wavelengths.

At low Galactic latitudes, the surveys include a large number of Galactic sources; therefore, the 4FGL class of $|b| < 10^{\circ}$ sources associated solely via the LR-method has been set to the "unknown" class as opposed to the "BCU" class used by default for sources at larger latitudes. These sources are thus not considered here.

3.3.2. Classification Based on the Broadband Spectral Energy Distribution

Blazars and more generally radio-loud AGNs can also be classified according to the peak photon frequency $\nu_{\rm s,peak}$ of the synchrotron part of their broadband SEDs. As a large number of 4LAC sources do not have a measured redshift (see Section 5.2), the frequency in the observer frame was used. The SEDs of all 4LAC AGNs were generated using the SED data archive and SED(t)-Builder interactive web-tool available at the Italian Space Agency (ASI) Space Science Data Center (SSDC).[75] Inspection of the error ellipse and the position of the counterpart was first performed using the Sky Data Explorer at SSDC. Two different approaches were followed to enable a cross-check. The first was the parametric procedure used in Abdo et al. (2010a) and Ackermann et al. (2011), which is based on the broadband spectral indices $\alpha_{\rm ro}$ (between 5 GHz and 5000 Å) and $\alpha_{\rm ox}$ (between 5000 Å and 1 keV). The list of surveys and catalogs providing the broadband flux density data is given in Abdo et al. (2010a). The second method, already used in 3LAC and favored here, consisted of fitting the SED synchrotron hump with a third-degree polynomial fit in the log-log plane. This fit was carried out manually on a source-by-source basis after carefully discarding outlying data (e.g., taken during flaring episodes) and those dominated by the thermal emission of the accretion disk or of the host galaxy. This methodology allowed us to assign a $\nu_{\rm s,peak}$ value to more objects, since a measured X-ray flux is not required, provided the SED curvature is sufficiently pronounced in the IR-optical band. This fit also provided the νF_{ν} value at the peak position. Limitations arose from possible human errors, the use of nonsimultaneous broadband synchrotron data, and remaining contamination of thermal emission. This contamination may result in an overestimation of the $\nu_{\rm s,peak}$ values for FSRQs, while the near-IR-optical contribution of the host galaxy may bias $\nu_{\rm s,peak}$ low in BL Lacs. Comparing the results of the two procedures indicated that the fitting method led to an average shift of -0.23 (rms: 0.53) and -0.22 (rms: 0.80) in $\log \nu_{\rm s,peak}$ relative to the initial method for FSRQs and BL Lacs, respectively. We identify these shifts as systematic uncertainties. Relative to 3LAC, a more conservative approach was followed when little data were available, leading to a lower fraction of classified sources. The mean differences in $\log \nu_{\rm s,peak}$ between 4LAC and 3LAC are -0.14 (rms: 0.37) and -0.11 (rms: 0.65) for FSRQs and BL Lacs, respectively.

Following Abdo et al. (2010a), the value of the observed $\nu_{\rm s,peak}$ was used to classify the source as either a low-synchrotron-peaked blazar (LSP, for sources with $\nu_{\rm s,peak} < 10^{14}$ Hz), an intermediate-synchrotron-peaked blazar (ISP, for 10^{14} Hz $< \nu_{\rm s,peak} < 10^{15}$ Hz), or a high-synchrotron-peaked blazar (HSP, if $\nu_{\rm s,peak} > 10^{15}$ Hz). To obtain the rest-frame value of $\nu_{\rm s,peak}$, a correction by a $(1+z)$ factor is needed, where z is the redshift.

4. The Fourth LAT AGN Catalog (4LAC)

Figure 1 displays the loci of the 4LAC sources in Galactic and J2000 equatorial coordinates. As already noted in previous LAC catalogs, it is clear from this figure that sources of different classes are not uniformly distributed over the sky. This anisotropy is demonstrated in Figure 2, showing the Galactic-latitude distributions for all 4LAC sources as well as for FSRQs, BL Lacs, and BCUs separately. The anisotropy is most noticeable for BL Lacs, which are 42% more abundant in the northern Galactic hemisphere than in the southern one. BCUs show the opposite pattern and somewhat offset the overall anisotropy as seen in the total distribution of sources, which is close to being uniform. The observed anisotropies stem from the larger and better spectroscopic data available in the literature for

[75] http://tools.ssdc.asi.it/SED/

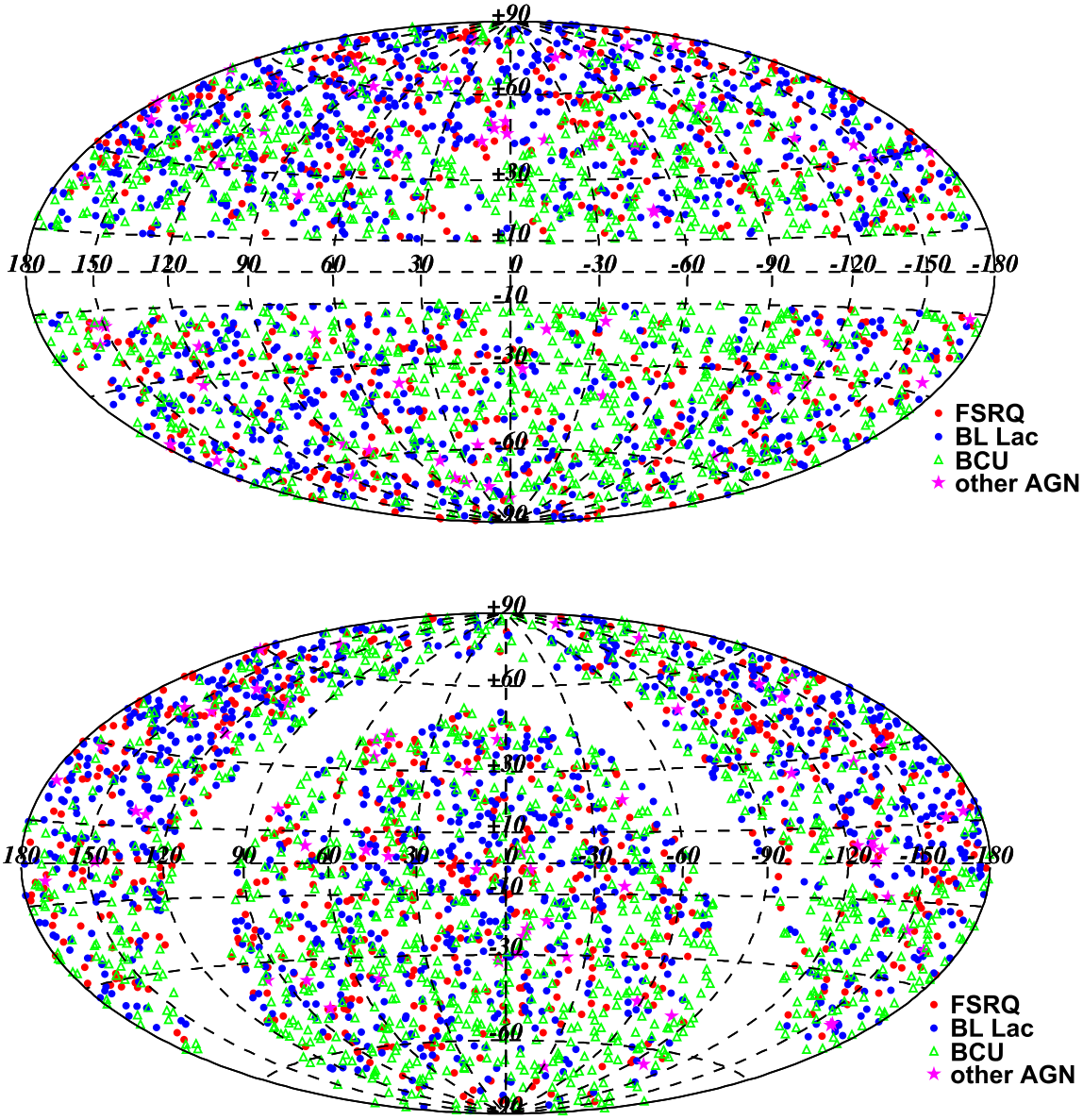

Figure 1. Locations of the sources in the Clean Sample in Galactic (top) and J2000 equatorial (bottom) coordinates and Hammer–Aitoff projection.

the northern hemisphere relative to the southern one. Better spectroscopic data are required to assess the BL Lac nature of an object relative to a FSRQ, because of the weaker optical emission lines in the spectrum of a BL Lac object.

The format of the 4LAC fits table is described in Table 3. In addition to relevant parameters[76] from the 4FGL fits file,[77] we report the optical and SED-based classes, redshifts, observer-frame synchrotron-peak frequencies, and νF_ν at the synchrotron-peak frequencies. When available, we also provide the VLBI and *Gaia* counterparts as given in the RFC. The median position accuracy of VLBI counterparts is 0.8 mas. Therefore, establishing association with VLBI immediately allows us to propagate the associations to the optical range using *Gaia* and IR using *WISE*. Following this route, we obtain *Gaia* associations with 2134 gamma-ray blazars (74%).

4.1. Census

Table 4 summarizes the 4LAC statistics. The 4LAC includes 2863 sources, with 655 FSRQs, 1067 BL Lacs, 1077 BCUs, and 64 other AGNs. A total of 1353 sources were not reported in the previous 3LAC catalog, although some of these have been reported elsewhere, e.g., Arsioli & Chang (2017) and Arsioli & Polenta (2018). The new sources include 204 FSRQs, 290 BL Lacs, 822 BCUs, and 36 nonblazar AGNs. The Clean Sample contains 2614 sources, with 591 FSRQs, 1027 BL Lacs, 941 BCUs, and 55 other AGNs. The figures shown in the following only include Clean Sample sources, unless specified otherwise

The SED-based scheme was able to classify 92% of the FSRQs and 85% of the BL Lacs in 4FGL. These values are lower than in 3LAC (99% and 97% for FSRQs and BL Lacs, respectively) due to the more conservative classification procedure used here. The classified fraction decreases to 60%

[76] The FSRQ 3C 454.3 is the only AGN whose preferred spectral shape is a power law with subexponential cutoff. The corresponding parameters can be found in the 4FGL fits file.

[77] https://fermi.gsfc.nasa.gov/ssc/data/access/lat/8yr_catalog/gll_psc_v20.fit

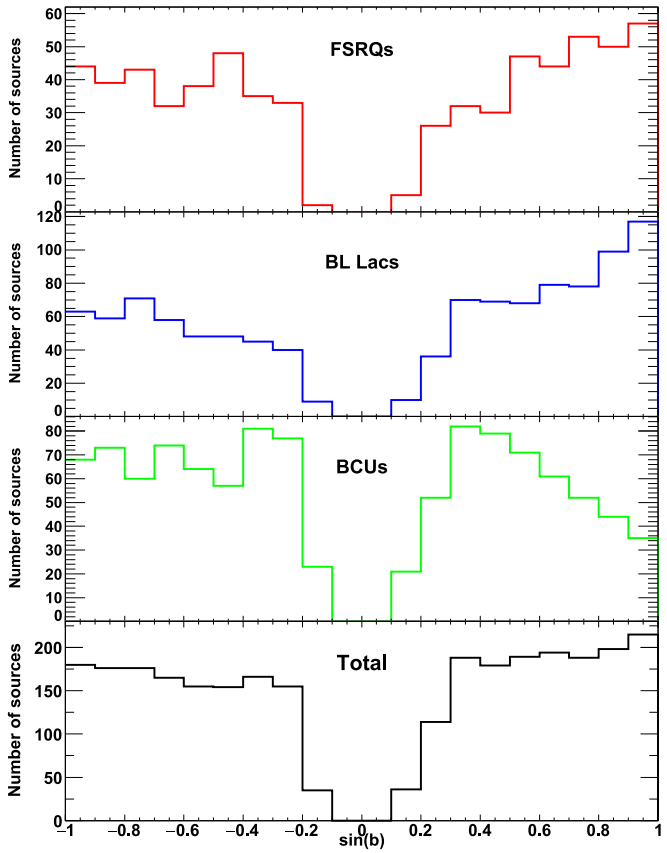

Figure 2. Distributions of Galactic latitudes for the different blazar classes.

for BCUs, for which fewer broadband archival data are available. Figure 3 shows the $\nu_{s,peak}$ distributions for the different classes. FSRQs are overwhelmingly of the LSP class; therefore, no distinction based on SED-based classes is made for them in figures and tallies. In addition to leaving more sources unclassified, the new procedure has produced a decrease in the the share of ISPs and HSPs among FSRQs, from 10% to 2%. Of the five HSP FSRQs, all located at $z < 0.63$, two are new: B3 0038 + 377 and PKS 1555−140.

BL Lacs are fairly evenly distributed among the LSP, ISP, and HSP subclasses. The 4LAC $\nu_{s,peak}$ distribution differs substantially from the 3LAC one, where HSPs were the most abundant subclass. The new classification procedure caused 15% of the AGN previously classified as HSP to be reclassified as ISP.

As a testimony to the substantial follow-up observational efforts already mentioned, 144 sources reported as BCUs in the 3LAC paper (either at high or low Galactic latitudes) are now classified as BL Lacs and 17 as FSRQs. Three BCUs have been reclassified as radio galaxies (IC 1531, TXS 0149+710, PKS 1304−215). Eight sources have changed from a FSRQ to a BL Lac (RGB J0250+172, NVSS J040324−242946, GB6 J0941+2721, 2MASS J11303636+1018245, PKS 1144−379, 4C +15.54, TXS 1951−115, PKS 2233−173) and three more from a BL Lac to a FSRQ (PMN J0709−0255, B2 2234+28A, TXS 2241+406).

The 3LAC sources that are not present in 4LAC are listed in Table 5, along with the various reasons for this situation. Fifty-five 3LAC sources have not been detected in 4FGL. Nineteen 3LAC sources were duplicate associations for which the smaller 4FGL error boxes relative to 3FGL have enabled the association ambiguity to be lifted. Fifteen sources reported in 3LAC have lost their associations (becoming unassociated), while three others are now associated with non-AGN counterparts, all due to improved localizations.

4.2. Nonblazar AGNs and Misaligned AGNs

Table 6 lists the 70 nonblazar AGNs included in the 4FGL, 64 of which belong to the 4LAC and 6 are part of the low-latitude sample. Nonblazar sources represent about 2% of the total number of AGNs in the 4FGL, a fraction that is basically identical to that found in the 3LAC. Nonblazar sources are further separated into six different classes: 41 radio galaxies,[78] 9 NLSy1s, 5 CSSs, 2 SSRQs, 1 Seyfert galaxy, and 11 other AGNs.

A total of 36 new nonblazar AGNs are reported in the 4LAC, 22 of which are radio galaxies. The median 1.4 GHz radio luminosity of the newly detected radio galaxies is about $10^{24.4}$ W Hz^{-1}, with the distribution ranging over more than 4 decades (from below 10^{22} W Hz^{-1}, for NGC 2892, to above 10^{26} W Hz^{-1}, for PKS 2324−02). The detection of the FR I radio galaxy 3C 120 in gamma-rays was first reported by Abdo et al. (2010c) using 15 months of LAT data, but it is reported in a LAT catalog for the first time. Its absence from previous catalogs can be attributed to periods of flaring interspersed with long periods of low activity (Tanaka et al. 2015). TXS 1303+114 and TXS 1516+064 are members of the FRICAT (Capetti et al. 2017a), although they were earlier proposed as candidate low-power BL Lacs in Capetti & Raiteri (2015) based on their mid-infrared and optical emission. Among the sources already present in previous LAT catalogs, Fornax A stands out because it is, for the first time, detected as an extended source (see Ackermann et al. 2016). Three 3FGL sources have changed class from BCU to radio galaxy (IC 1531, TXS 0149+710, and PKS 1304−215). We associate 4FGL J1346.3−6026 with Cen B, although its location is not coincident with that of the radio-galaxy core but points to the southern radio jet. Similarly, we associate 4FGL J1516.5+0015 with the radio galaxy 4C +00.56 (PKS 1514+00, $z = 0.0525$) while the gamma-ray position is closer to the lobes than to the core of the radio galaxy.

The only new SSRQ is 3C 212, for which X-ray emission associated with both lobes was detected by *Chandra* (Aldcroft et al. 2003). Three new CSSs are reported in the 4LAC: 3C 138, 3C 216, and 3C 309.1. These new CSSs are hosted in quasars. At the pc scale, they show a core-jet structure with apparent superluminal motion, indicating Doppler effects and small viewing angles (Paragi et al. 2000; Shen et al. 2001; Lister et al. 2019). While the CSSs all have very high radio luminosity, at the opposite end of the radio luminosity distribution are two other new LAT sources, NGC 3894 and NGC 6328. Based on the small extent of their radio emission, two-sided parsec scale morphology (Taylor et al. 1998; Tingay & de Kool 2003), and low radio luminosity, these sources are excellent candidates for being young radio galaxies (see also Migliori et al. 2016; Principe et al. 2019).

The classification of a source as an NLSy1 relies on three criteria, as reported in Osterbrock & Pogge (1985), Goodrich (1989), and Pogge (2000): (i) a full width half maximum (FWHM) of the H_β line <2000 km s^{-1}; (ii) a [O III]λ5007/H_β ratio <3; and (iii) unusually strong Fe II lines. Nine NLSy1 are reported in the 4LAC. Four of them are new with respect to

[78] Two different gamma-ray sources are associated with the core and lobes of Cen A.

Table 3
4LAC FITS Format

Column	Format	Unit	Description
Source_Name	18A	⋯	Source name 4FGL JHHMM.m+DDMMa[a]
RAJ2000	E	deg	R.A.
DEJ2000	E	deg	Decl.
GLON	E	deg	Galactic Longitude
GLAT	E	deg	Galactic Latitude
Signif_Avg	E	⋯	Source significance in σ units over the 50 MeV–1 TeV band
Flux1000	E	cm^{-2} s^{-1}	Integral photon flux from 1 to 100 GeV
Unc_Flux1000	E	cm^{-2} s^{-1}	1σ error on integral photon flux from 1 to 100 GeV
Energy_Flux100	E	erg cm^{-2} s^{-1}	Energy flux from 100 MeV to 100 GeV obtained by spectral fitting
Unc_Energy_Flux100	E	erg cm^{-2} s^{-1}	1σ error on energy flux from 100 MeV to 100 GeV
SpectrumType	17A	⋯	Spectral type in the global model (PowerLaw, LogParabola, PLSuperExpCutoff)
PL_Index	E	⋯	Photon index when fitting with PowerLaw
Unc_PL_Index	E	⋯	1σ error on PL_Index
Pivot_Energy	E	MeV	Pivot Energy
LP_Index	E	⋯	Photon index at Pivot_Energy (α) when fitting with LogParabola
Unc_LP_Index	E	⋯	1σ error on LP_Index
LP_beta	E	⋯	Curvature parameter (β) when fitting with LogParabola
Unc_LP_beta	E	⋯	1σ error on LP_beta
Flags	I	⋯	Analysis flags
CLASS	6A	⋯	Class designation for associated source
ASSOC1	30A	⋯	Name of identified or likely associated source
ASSOC_PROB_BAY	E	⋯	Probability of association according to the Bayesian method
ASSOC_PROB_LR	E	⋯	Probability of association according to the Likelihood Ratio method
Counterpart_Catalog	10A		Counterpart catalog driving the association
RA_Counterpart	D	deg	R.A. of the counterpart ASSOC1
DEC_Counterpart	D	deg	Decl. of the counterpart ASSOC1
Unc_Counterpart	E	deg	95% precision of the counterpart localization
VLBI_Counterpart	14A	⋯	Name of the VLBI counterpart
Gaia_Counterpart	29A	⋯	Name of the *Gaia* counterpart established via the VLBI position
Gaia_G_Magnitude	E	⋯	Gaia Magnitude at the *G* band
Redshift	E	⋯	Redshift
SED_class	6A	⋯	SED-based class
nu_syn	E	Hz	Synchrotron-peak frequency in observer frame
nuFnu_syn	E	erg cm^{-2} s^{-1}	Spectral energy distribution at synchrotron-peak frequency
Variability_Index	E	⋯	Variability index
Frac_Variability	E	⋯	Fractional variability
Unc_Frac_Variability	E	⋯	1σ error on fractional variability
Highest_energy	E	GeV	Energy of the highest-energy ULTRACLEANVETO photon with association probability $P > 0.95$

Note.
[a] The coordinates are rounded, following the IAU convention.
(This table is available in its entirety in machine-readable form.)

the 3LAC: 1ERS B1303+515, B3 1441+476, MG2 J164443 +2618, and TXS 2116−077. B3 1441+476, MG2 J164443 +2618, and TXS 2116−077 were previously reported by D'Ammando et al. (2015a) and Paliya et al. (2018), respectively. The Circinus galaxy (Hayashida et al. 2013) remains the only radio-quiet Seyfert galaxy detected by the LAT.

Among other AGNs, there are two remarkable cases. One is PKS 0521−36, previously classified as BCU in the 3LAC, which shows a knotty VLBA radio structure similar to misaligned AGN. Based on the broad emission lines in the optical and ultraviolet bands and the steep radio spectrum, a possible classification as an intermediate object between broad-line radio galaxies and SSRQ has been suggested by D'Ammando et al. (2015b). The new source PKS 2331−240 was the subject of a multiwavelength study revealing features of a giant radio galaxy restarted as a blazar (Hernández-García et al. 2017).

Finally, 10 nonblazar AGNs reported in the 3LAC are not confirmed in the 4LAC. Five of them had a double association in the 3LAC and are now firmly associated with the other counterpart; two have changed associations (formerly with 3C 221 and 3C 275.1); one has been reclassified as a BCU (GB 1310+487); while two 3FGL nonblazar AGNs are missing in 4FGL (TXS 0348+013, PKS 1617−251).

4.3. Low-latitude AGNs

In addition to high-latitude ($|b| > 10°$) 4LAC sources, we present a low-latitude sample. This sample is less complete than the 4LAC because the LAT detection flux limit is higher

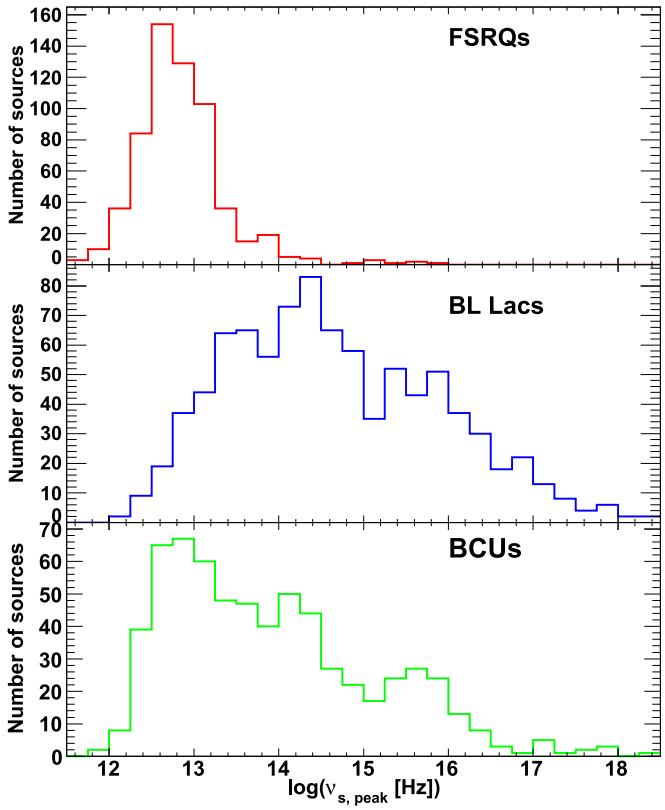

Figure 3. Distributions of the synchrotron peak frequency $\nu_{s,peak}$ for the different blazar classes.

Table 4
Census of Sources

AGN type	Entire 4LAC	4LAC Clean Sample[a]	Low-latitude Sample
All	2863	2614	344
FSRQ	655	591	36
LSP	587	540	34
ISP	11	9	0
HSP	5	4	0
No SED classification	52	38	2
BL Lac	1067	1027	64
LSP	297	288	15
ISP	280	270	7
HSP	326	316	25
No SED classification	164	153	17
Blazar of unknown type	1077	941	238
LSP	382	327	57
ISP	142	128	9
HSP	128	126	12
No SED classification	425	360	160
Nonblazar AGN	64	55	6
NLSy1	9	9	0
RG	38	31	4
CSS	5	5	0
SSRQ	2	2	0
SEY	0	0	1
Other AGN	10	8	1

Note.
[a] Sources with single counterparts and without analysis flags. See Section 3.2 for the definitions of this sample.

Table 5
The 3LAC Sources Not Present in 4LAC

3FGL Name	Counterpart	Class	4FGL[a]
J0127.9+2551	4C +25.05	fsrq	M
J0135.0+6927	TXS 0130+691	bcu	M
J0211.7+5402	TXS 0207+538	bcu	M
J0216.1-7016	PMN J0215-7014	bcu	M
J0217.3+6209	TXS 0213+619	bcu	M
J0223.5+6313	TXS 0219+628	bcu	M
J0228.5+6703	GB6 J0229+6706	bcu	M
J0302.0+5335	GB6 J0302+5331	bcu	M
J0336.9-1304	PKS 0334-131	fsrq	M
J0351.1+0128	TXS 0348+013	ssrq	M
J0512.2+2918	B2 0509+29	bcu	M
J0514.4+5603	TXS 0510+559	fsrq	M
J0517.4+4540	4C +45.08	fsrq	M
J0528.3+1815	1RXS J052829.6+181657	bcu	M
J0618.9-1138	TXS 0616-116	bcu	M
J0627.9-1517	NVSS J062753-152003	bcu	M
J0730.3+6720	GB6 J0731+6718	fsrq	M
J0742.4-8133	SUMSS J074220-813139	bcu	M
J0744.1-3804	PMN J0743-3804	bcu	M
J0904.9+2739	GB6 J0905+2748A	fsrq	M
J0928.7+7300	GB6 J0929+7304	bcu	M
J0956.7-6441	AT20G J095612-643928	bcu	M
J1005.0-4959	PMN J1006-5018	bcu	M
J1016.0-0635	NVSS J101626-063624	bcu	M
J1024.8+0105	PMN J1024+0056	bcu	M
J1037.4-3742	PKS 1034-374	fsrq	M
J1123.2-6415	AT20G J112319-641735	bcu	M
J1205.4+0412	MG1 J120448+0408	fsrq	M
J1218.5+6912	NVSS J122044+690522	bcu	M
J1326.1+2931	TXS 1323+298	bll	M
J1330.0-3818	Tol 1326-379	fsrq	M
J1356.3-4029	SUMSS J135625-402820	bcu	M
J1415.0-1001	PKS B1412-096	fsrq	M
J1509.9-2951	TXS 1507-296	bcu	M
J1513.1-1014	PKS 1511-100	fsrq	M
J1514.1+2940	MG2 J151421+2930	fsrq	M
J1536.6+8331	NVSS J153556+832614	bcu	M
J1541.8+1105	MG1 J154207+1110	fsrq	M
J1621.1-2331	PKS 1617-235	agn	M
J1645.2-5747	AT20G J164513-575122	bcu	M
J1648.5-4829	PMN J1648-4826	bcu	M
J1723.5-5609	PMN J1723-5614	bcu	M
J1747.1+0139	PMN J1746+0141	bcu	M
J1757.4+6536	7C 1757+6536	bcu	M
J1804.1+0341	TXS 1801+036	fsrq	M
J1819.1+4259	NVSS J181927+425800	bcu	M
J1822.1-7051	PMN J1823-7056	bcu	M
J1949.4-6140	PMN J1949-6137	bcu	M
J2107.7-4822	PMN J2107-4827	bcu	M
J2151.6-2744	PMN J2151-2742	fsrq	M
J2203.7+3143	4C +31.63	fsrq	M
J2236.2-5049	SUMSSJ223605-505521	bcu	M
J2246.2+1547	NVSS J224604+154437	bcu	M
J2305.3-4219	SUMSS J230512-421859	bcu	M
J2343.6+1551	MG1 J234342+1542	fsrq	M
J0003.8-1151	PKS 0001-121	bcu	D
J0009.1+0630	GB6 J0009+0625	bll	D
J0059.1-5701	PKS 0056-572	bcu	L
J0203.6+3043	B2 0200+30	fsrq	D
J0426.6+0459	4C +04.15	bcu	L
J0442.6-0017	1RXS J044229.8-001823	bll	D
J0447.8-2119	PKS 0446-212	fsrq	L

Table 5
(Continued)

3FGL Name	Counterpart	Class	4FGL[a]
J0515.3-4557	PMN J0514-4554	bcu	D
J0526.0+4253	NVSS J052520+425520	bcu	C
J0542.2-8737	SUMSS J054923-874001	bcu	L
J0618.0+7819	1REX J061757+7816.1	fsrq	C
J0647.1-4415	SUMSS J064648-441929	bcu	C
J0712.2-6436	MRC 0712-643	bcu	L
J0744.8-4028	PMN J0744-4032	bcu	L
J0807.9+4946	SDSS J080754.50+494627.6	fsrq	D
J0824.9+3916	4C +39.23B	css	D
J0825.4-0213	PMN J0825-0204	bcu	L
J0934.1+3933	3C 221	rdg	D
J1007.4-3334	TXS 1005-333	bcu	D
J1010.8-0158	NVSS J101051-020227	fsrq	D
J1018.1+1904	MG1 J101810+1903	bcu	D
J1048.6+2338	NVSS J104900+233821	bll	C
J1101.5+4106	B3 1058+413	bcu	D
J1146.8+3958	NVSS J114653+395751	bcu	D
J1207.6-4537	PMN J1207-4531	bcu	L
J1244.1+1615	3C 275.1	ssrq	D
J1256.7+5328	TXS 1254+538	bcu	L
J1300.2+1416	NVSS J130041+141728	bcu	D
J1322.8-0938	PMN J1323-0943	bcu	D
J1451.2+6355	TXS 1450+641	bcu	D
J1514.8+4446	NVSS J151436+445003	fsrq	L
J1554.4+2010	1ES 1552+203	bll	L
J1617.3-2519	TXS 1613-251	agn	D
J1625.9+4125	4C +41.32	fsrq	D
J1908.8-0130	NVSS J190836-012642	bcu	L
J2036.8-2830	PMN J2036-2830	fsrq	L
J2110.3+3540	B2 2107+35A	bcu	L
J2348.4-5100	SUMSS J234852-510311	bcu	L

Note.
[a] M: missing gamma-ray source in 4FGL. L: 3FGL source present in 4FGL but now unassociated. C: 3FGL source present in 4FGL but now associated with a non-AGN counterpart. D: duplicate counterpart in 3LAC now missing in 4LAC.

(This table is available in machine-readable form.)

in this region (by factors of a few) and the counterpart catalogs suffer from Galactic extinction. Because a large contamination of Galactic sources is present in the radio and X-ray surveys used in the LR association method, the classes of the resulting associations are highly uncertain. Consequently, these associations were not considered here. The census of the low-latitude sample is given in the last column of Table 4. The fraction of BCUs (62%) is overwhelming, as expected from the observational hindrance mentioned above.

5. Properties of the 4LAC Clean Sample Sources

5.1. Flux and Spectral Properties

Although many 4FGL/4LAC sources show significant spectral curvature in the gamma-ray band (The Fermi-LAT collaboration 2020), the gamma-ray power-law photon index, Γ, represents a convenient way to compare the spectral hardness of different sources across various classes and flux values. This index is plotted versus the 8 yr average energy flux above 100 MeV, S_{25}, in Figure 4. The flux detection limit ranges from (1–4) $\times 10^{-12}$ erg cm^{-2} s^{-1} (i.e., close to 1 eV cm^{-2} s^{-1}), with a slight dependence on the spectral hardness. This dependence is stronger than in 3LAC due to the introduction of weights in the 4FGL likelihood to better account for systematic uncertainties. BCUs are rare among the brightest sources (i.e., with $S_{25} > 10^{-11}$ erg cm^{-2} s^{-1}), while they are dominant close to the flux limit.

Figure 5 displays the photon index distributions for the different optical blazar classes, for 4LAC sources already present in 3LAC and the new ones. Newly detected gamma-ray FSRQs, i.e., not reported in previous LAT AGN catalogs, have somewhat softer spectra (difference in median $\Gamma \simeq 0.08$) than the previously reported ones, possibly indicating the emergence of sources with SED peaking at lower energy. The difference between the FSRQ and BL Lac distributions is striking. The Γ medians and rms are 2.44 ± 0.20 and 2.02 ± 0.21 for FSRQs and BL Lacs respectively. The relative separation in gamma-ray spectral hardness between FSRQs and BL Lacs already reported in previous LAT catalogs is confirmed: 89% of FSRQs and 86% of BL Lacs have Γ greater and lower than 2.25, respectively. This feature by itself carries significant discrimination power between the two classes. The photon index varies among the BL Lac subclasses, with medians and rms in Γ of 2.17 ± 0.16, 2.05 ± 0.19, and 1.88 ± 0.14 for LSPs, ISPs, and HSPs, respectively. The BCU index distribution straddles that of the two classes and extends to $\Gamma = 3$. The expectation that both the BCU photon-index and $\nu_{\rm s,peak}$ distributions correspond to linear combinations of the observed FSRQ and BL Lac distributions is tested in Figure 6. Composite distributions were built assuming the same fractions of FSRQs and BL Lacs as in the observed sample for the photon index distributions. For the $\nu_{\rm s,peak}$ distribution, a slight correction (a factor of 0.92) in the normalization was introduced in disfavor of FSRQ to account for the difference in efficiency for fitting the SEDs successfully, due to better broadband data for FSRQs (see Section 4.1). The reasonable agreement between the composite and BCU distributions for both photon index and $\nu_{\rm s,peak}$ seen in Figure 6 supports the idea that the sample of unclassified blazars (i.e., BCUs) is of a composition similar to that of the classified sample in 4LAC.

Figure 7 displays the photon index as a function of the observed synchrotron peak frequency. Even though $\nu_{\rm s,peak}$ should be corrected by a factor $1+z$ to obtain the rest-frame value and make the correlation more physical, the fairly strong correlation already noted in previous catalogs is clearly visible. The correlation obtained in 3LAC was reproduced theoretically by Dermer et al. (2015) using an equipartition blazar model with a log-parabola description of the electron energy distribution. In the region of $\nu_{\rm s,peak}$ where BL Lac LSPs and FSRQs overlap, their photon index distributions are very similar. This is the expected region for objects that might be transitioning between being FSRQs and BL Lacs. Ruan et al. (2014) found six such transitioning objects. Five of them, all of the LSP subclass, are present in 4LAC: OJ 451 (4FGL J0833.9+4223, FSRQ, $\Gamma = 2.44 \pm 0.07$), TXS 1013+054 (4FGL J1016.0+0512, FSRQ, $\Gamma = 2.18 \pm 0.04$), PKS 1247+025 (4FGL J1250.6 +0217, BLL, $\Gamma = 2.00 \pm 0.10$), 5C 12.291 (4FGL J1308.5 +3547, FSRQ, $\Gamma = 2.29 \pm 0.06$), and PMN J2206−0031 (4FGL J2206.8−0032, BLL, $\Gamma = 2.25 \pm 0.05$). Three of these sources have Γ very close to the $\Gamma = 2.25$ limit outlined above. The four HSP FSRQs in the Clean Sample all have $\Gamma < 2.02$, as expected from the class of "HFSRQs," which is not fitting with the "blazar sequence" (see, e.g., Padovani 2007).

Table 6
Nonblazar Objects and Misaligned AGNs

4FGL Name	Name	Type	Photon Index	Redshift/Distance (Mpc)
J0009.7-3217	IC 1531	rdg	2.2 ± 0.14	93.4[a]
J0013.6+4051	4C +40.01	agn	2.21 ± 0.14	0.255
J0038.7-0204	3C 17	rdg	2.81 ± 0.11	0.22
J0057.7+3023	NGC 315	rdg	2.35 ± 0.11	0.016
J0237.7+0206	PKS 0235+017	rdg	2.17 ± 0.18	0.022
J0308.4+0407	NGC 1218	rdg	2.0 ± 0.06	0.029
J0312.9+4119	B3 0309+411B	rdg	2.47 ± 0.19	0.136
J0316.8+4120	IC 310	rdg	1.78 ± 0.18	0.019
J0319.8+4130	NGC 1275	rdg	2.12 ± 0.01	0.69[a]
J0322.6-3712e	Fornax A	rdg	2.05 ± 0.07	17.8[a]
J0324.8+3412	1H 0323+342	nlsy1	2.82 ± 0.04	0.061
J0334.3+3920	4C +39.12	rdg	1.9 ± 0.13	0.021
J0433.0+0522	3C 120	rdg	2.72 ± 0.05	0.033
J0519.6-4544	Pictor A	rdg	2.46 ± 0.13	0.035
J0521.2+1637	3C 138	css	2.37 ± 0.13	0.759
J0522.9-3628	PKS 0521-36	agn	2.45 ± 0.01	0.056
J0627.0-3529	PKS 0625-35	rdg	1.9 ± 0.04	0.055
J0708.9+4839	NGC 2329	rdg	1.95 ± 0.18	0.019
J0758.7+3746	NGC 2484	rdg	2.01 ± 0.16	171[a]
J0840.8+1317	3C 207	ssrq	2.48 ± 0.1	0.681
J0850.0+5108	SBS 0846+513	nlsy1	2.27 ± 0.02	0.583
J0858.1+1405	3C 212	ssrq	2.52 ± 0.15	1.048
J0910.0+4257	3C 216	css	2.52 ± 0.11	0.67
J0931.9+6737	NGC 2892	rdg	2.23 ± 0.06	0.023
J0948.9+0022	PMN J0948+0022	nlsy1	2.64 ± 0.02	0.585
J1012.7+4228	B3 1009+427	agn	1.76 ± 0.09	0.365
J1116.6+2915	B2 1113+29	rdg	1.44 ± 0.24	0.047
J1118.2-0415	PMN J1118-0413	agn	2.64 ± 0.08	…
J1144.9+1937	3C 264	rdg	1.94 ± 0.1	0.022
J1149.0+5924	NGC 3894	rdg	2.06 ± 0.12	46.9[a]
J1230.8+1223	M87	rdg	2.06 ± 0.04	16.5[a]
J1305.3+5118	IERS B1303+515	nlsy1	2.85 ± 0.17	0.788
J1306.3+1113	TXS 1303+114	rdg	1.95 ± 0.18	0.086
J1306.7-2148	PKS 1304-215	rdg	2.13 ± 0.09	0.126
J1325.5-4300	Cen A	rdg	2.65 ± 0.02	3.8[a]
J1331.0+3032	3C 286	css	2.41 ± 0.14	0.85
J1356.2-1726	PKS B1353-171	agn	2.08 ± 0.15	0.075
J1443.1+5201	3C 303	rdg	1.98 ± 0.15	0.141
J1443.1+4728	B3 1441+476	nlsy1	2.56 ± 0.11	0.705
J1449.5+2746	B2 1447+27	rdg	1.54 ± 0.18	0.031
J1449.7-0910	1RXS J144942.2-091018	agn	2.04 ± 0.18	…
J1459.0+7140	3C 309.1	css	2.45 ± 0.09	0.91
J1505.0+0326	PKS 1502+036	nlsy1	2.59 ± 0.04	0.409
J1516.5+0015	PKS 1514+00	rdg	2.59 ± 0.11	0.052
J1518.6+0614	TXS 1516+064	rdg	1.86 ± 0.17	0.102
J1521.1+0421	PKS B1518+045	rdg	2.06 ± 0.15	0.052
J1543.6+0452	CGCG 050-083	agn	1.87 ± 0.08	0.04
J1630.6+8234	NGC 6251	rdg	2.35 ± 0.03	98.2[a]
J1644.9+2620	MG2 J164443+2618	nlsy1	2.78 ± 0.1	0.144
J1724.2-6501	NGC 6328	rdg	2.49 ± 0.18	0.014
J1829.5+4845	3C 380	css	2.43 ± 0.03	0.695
J1843.4-4835	PKS 1839-48	rdg	1.99 ± 0.17	0.111
J2007.9-4432	PKS 2004-447	nlsy1	2.6 ± 0.05	0.24
J2114.8+2026	TXS 2112+202	agn	2.13 ± 0.16	…
J2118.8-0723	TXS 2116-077	nlsy1	2.83 ± 0.15	0.26
J2156.0-6942	PKS 2153-69	rdg	2.83 ± 0.11	0.028
J2227.9-3031	PKS 2225-308	rdg	1.99 ± 0.17	0.056
J2302.8-1841	PKS 2300-18	rdg	2.17 ± 0.15	0.129
J2326.9-0201	PKS 2324-02	rdg	2.44 ± 0.14	0.188
J2329.7-2118	PKS 2327-215	rdg	2.45 ± 0.16	0.031
J2334.9-2346	PKS 2331-240	agn	2.42 ± 0.12	0.048
J2338.1+0325	PKS 2335+03	agn	2.36 ± 0.15	0.27
J2341.8-2917	PKS 2338-295	rdg	2.24 ± 0.15	0.052

Table 6
(Continued)

4FGL Name	Name	Type	Photon Index	Redshift/Distance (Mpc)
J0153.4+7114	TXS 0149+710	rdg	1.9 ± 0.11	0.022
J0418.2+3807	3C 111	rdg	2.71 ± 0.06	0.05
J1236.9-7232	PKS 1234-723	rdg	2.36 ± 0.14	0.024
J1346.3-6026	Cen B	rdg	2.4 ± 0.05	0.013
J1413.1-6519	Circinus galaxy	sey	2.25 ± 0.1	4.0[a]
J1824.7-3243	PKS 1821-327	agn	2.23 ± 0.12	0.355

Note. The table includes the nonblazar objects and MAGNs at high latitudes (top) and low latitudes (bottom) associated with 4FGL sources (Cen A Core and Cen A Lobes constitute a single object).
[a] Indicates that the value is the distance in Mpc.

(This table is available in machine-readable form.)

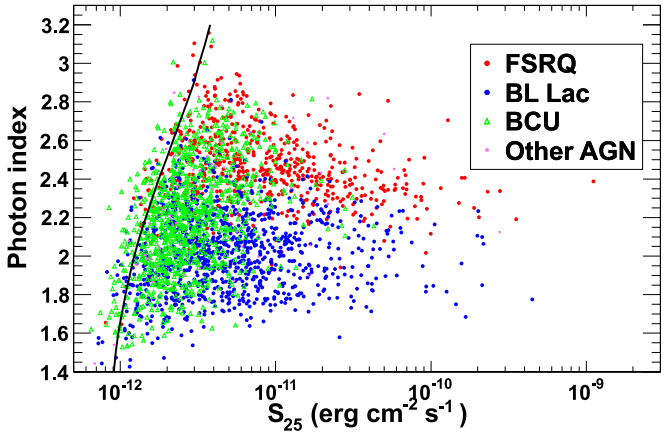

Figure 4. Photon index as a function of energy flux above 100 MeV. Curve represents the approximate detection limit. Error bars have been omitted for clarity. Mean photon-index uncertainties are 0.08, 0.10, and 0.14 for FSRQs, BL Lacs, and BCUs, respectively.

Some blazars have undergone statistically significant spectral changes since 3LAC: PKS 1349−439 (BL Lac, $\Delta\Gamma \equiv \Gamma_{4FGL} - \Gamma_{3FGL} = -0.37 \pm 0.12$), RX J1415.5+4830 (BL Lac, $\Delta\Gamma = -0.70 \pm 0.16$), PKS 1532+01 (FSRQ, $\Delta\Gamma = -0.41 \pm 0.12$), and S4 1800+44 (FSRQ, $\Delta\Gamma = -0.33 \pm 0.09$). The changes in photon index are all such that Γ_{4FGL} is closer to the median of the class than was Γ_{3FGL}. Inspection of the light curves reveals that all four sources show enhanced activity in the last 4 yr of the 4LAC period relative to that of 3LAC, which may be correlated with the observed spectral hardening. Fourteen other sources have experienced spectral variations greater than 3σ but of lower amplitudes than these four.

As noted above, many FSRQs and BL Lacs show significant spectral curvature. The comparison of the TS distributions of sources with significantly curved spectra to those of the whole sample of FSRQs and BL Lacs (Figure 8) demonstrates that essentially all bright blazars have curved spectra in the LAT energy range. A total of 212 FSRQs, 172 BL Lacs, and 70 BCUs have significantly curved spectra. To enable comparison, if we apply the more stringent threshold on the curvature significance (i.e., approximately 4σ instead of 3σ) used in 3LAC, these numbers become 146 FSRQs, 112 BL Lacs, and 26 BCUs. In 3LAC, the comparable numbers were 57, 32, and 8, respectively. It is therefore likely that fainter blazars have curved spectra as well, but the current data do not allow their curvature to be established with high confidence.

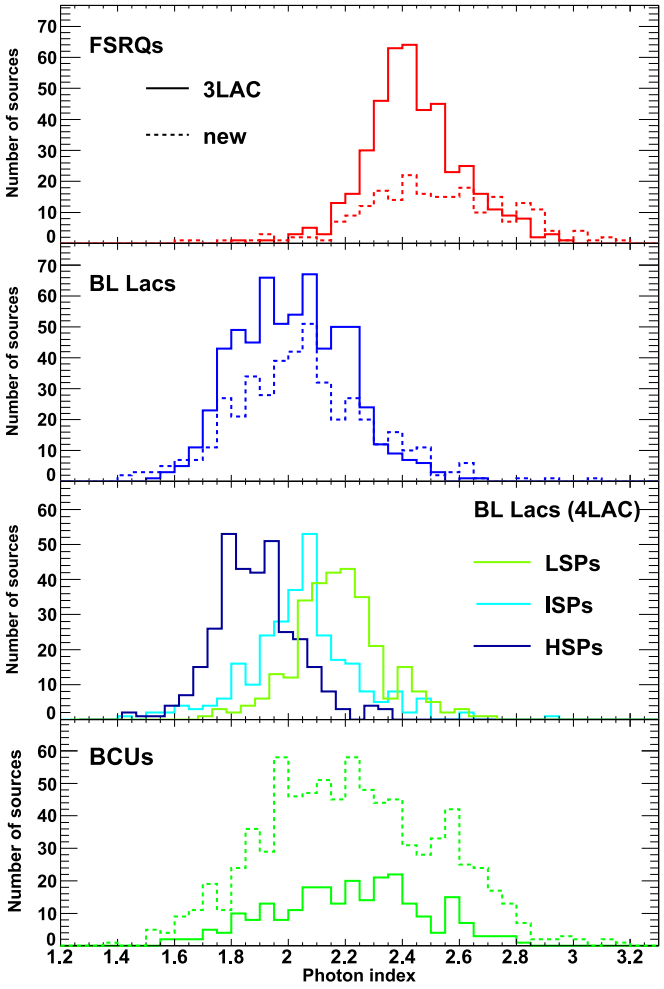

Figure 5. Photon index distributions for the different blazar classes and subclasses. In the top, second from top, and bottom panels, the solid histograms represent the 4LAC sources already present in 3LAC and the dashed histograms the new 4LAC sources.

5.2. Redshifts

We conducted a literature search for spectroscopic redshifts. Well-established redshifts (999) came from BZCAT or the optical campaigns mentioned in Section 3.3.1. For the other sources (656), remaining contamination from photometric values or from bad signal-to-noise ratio optical spectra cannot be excluded. We found redshifts for all the FSRQs, but were unable to find those for 36% of the BL Lacs in our sample

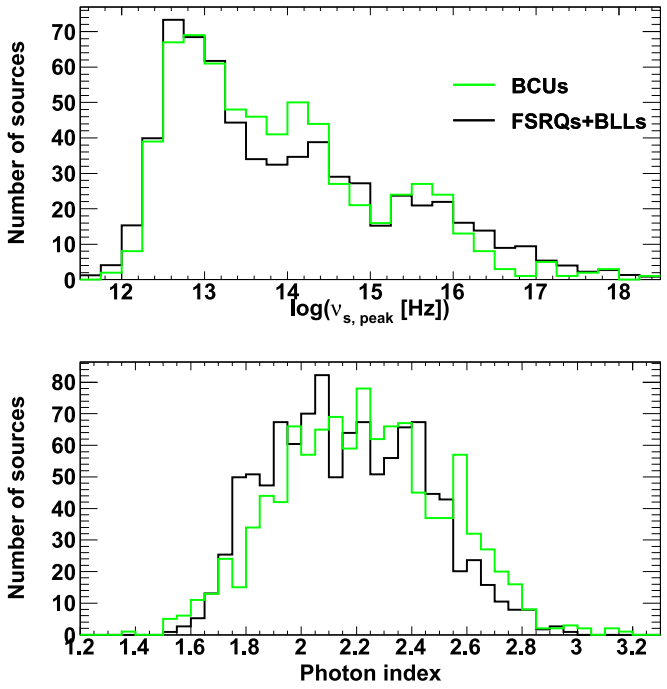

Figure 6. Comparison between the $\nu_{s,peak}$ (top) and photon index (bottom) distributions of BCUs (green) and the (normalized) distributions obtained by adding up the FSRQ and BL Lac distributions (black). See text for details.

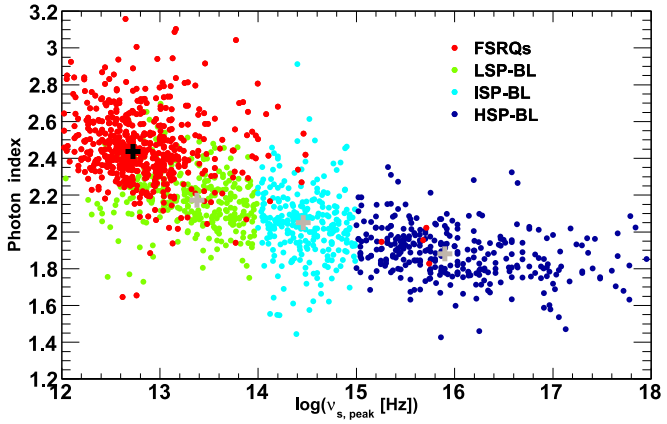

Figure 7. Photon index vs. frequency of the synchrotron peak $\nu_{s,peak}$ in the observer frame. Error bars have been omitted for clarity. The mean photon-index uncertainties are 0.08 and 0.10 for FSRQs and BL Lacs, respectively. Black cross depicts the FSRQ median photon index, while gray crosses depict those for the three BL Lac subclasses.

(compared to 50% of the BL Lacs without redshifts in 3LAC). This clear improvement has been primarily achieved thanks to follow-up observations of 3LAC blazars (see Section 3.3.1 for references). The fraction without redshifts is similar for the three BL Lac subclasses (41%, 42%, and 28% for LSPs, ISPs, and HSPs, respectively).

The redshift distributions are displayed in Figure 9 for FSRQs and BL Lacs. The FSRQ distribution shows a broad peak around $z = 1$. This trend confirms the conclusion that the number density of FSRQs grows dramatically up to redshift $\simeq$0.5–2.0 and declines thereafter (Ajello et al. 2012). For BL Lacs, the overall peak lies at $z \simeq 0.3$. For the sake of comparison, the distributions for previously and newly reported AGNs are plotted separately. The redshifts of the 3LAC and newly detected blazars are similar, with respective medians and

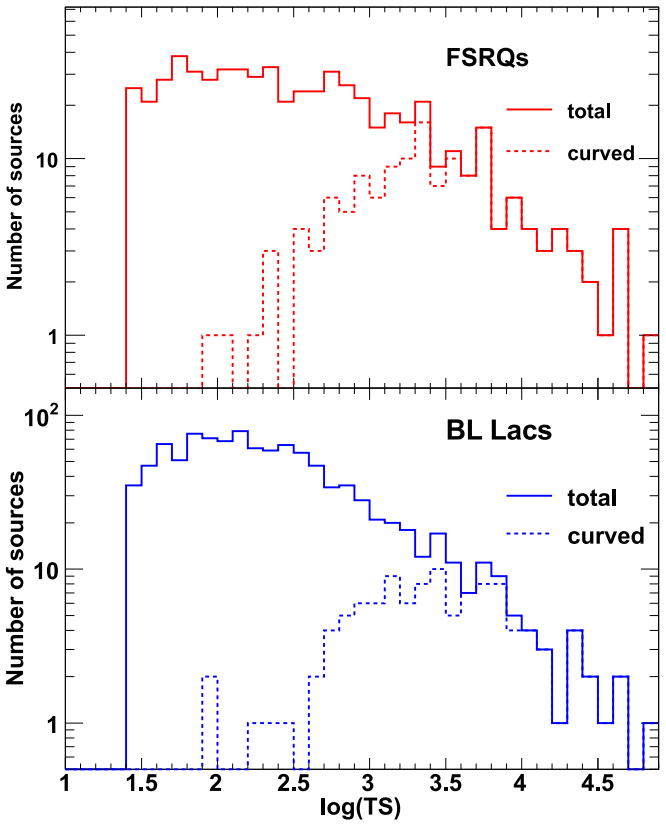

Figure 8. TS distributions of FSRQs (top) and BL Lacs (bottom) for curved-spectra sources and the whole sample.

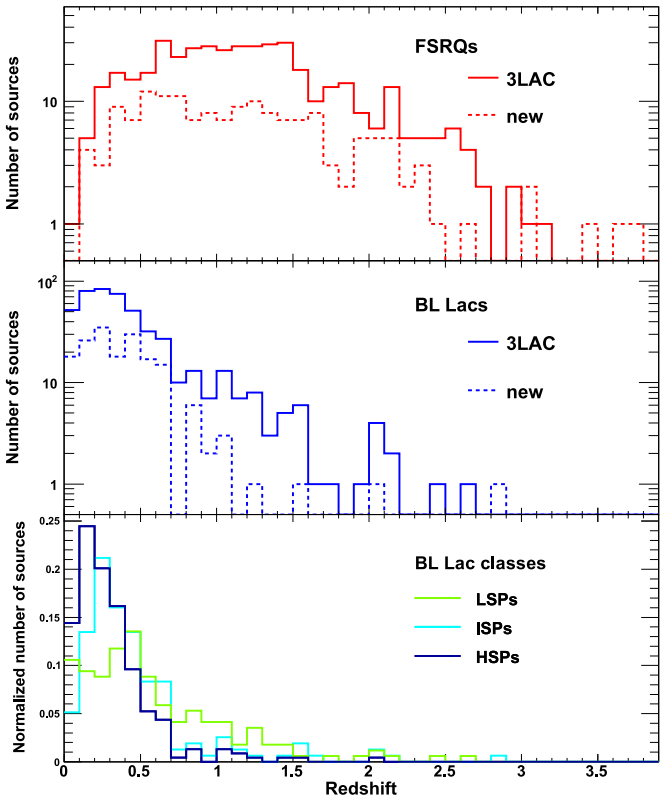

Figure 9. Redshift distributions, where solid lines indicate 4LAC sources also in 3LAC and dashed lines signify new 4LAC sources, for FSRQs (top) and BL Lacs (bottom).

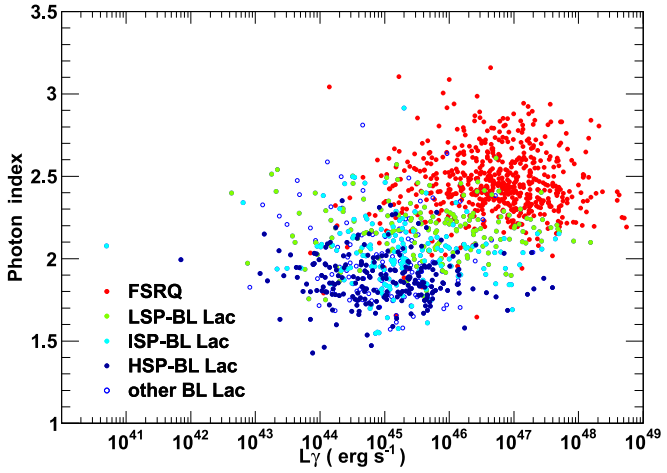

Figure 10. Photon index vs. gamma-ray luminosity for the different blazar classes and subclasses. Error bars have been omitted for clarity. Mean photon-index uncertainties are 0.08 and 0.10 for FSRQs and BL Lacs, respectively.

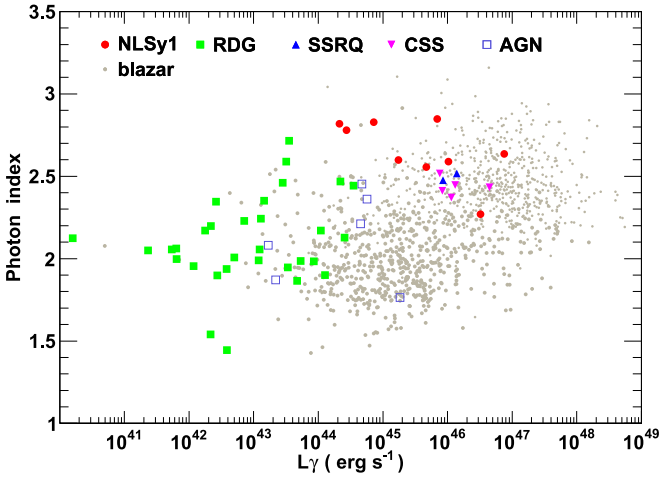

Figure 11. Photon index vs. gamma-ray luminosity for the different nonblazar classes. Blazars are included for comparison and depicted in gray regardless of their classes. Error bars have been omitted for clarity. Mean photon-index uncertainty is 0.11 for the nonblazar AGNs.

widths of 1.14 ± 0.62 and 1.09 ± 0.68 for FSRQs, and of 0.34 ± 0.42 and 0.36 ± 0.34 for BL Lacs. The median redshifts decrease between BL Lac LSPs, ISPs, and HSPs from 0.47 to 0.36 to 0.25, respectively. While the maximum redshift for an FSRQ was 3.1 in earlier LAC catalogs, five counterparts to 4LAC sources have higher redshifts: GB 1508+5714 ($z = 4.31$), PKS 1351−018 ($z = 3.72$), PKS 0335−122 ($z = 3.44$), MG3 J163554+3629 ($z = 3.65$), and PMN J0833−0454 ($z = 3.45$). GB 1508+5714 and PKS 0335−122 are not present in the Clean Sample, however, due to analysis flags. The detections of three of these sources (PKS 1351−018, GB 1508+5714, MG3 J163554+3629 were reported earlier in Ackermann et al. (2017). Two other high-z sources (NVSS J064632+445116 and NVSS J212912-153841), whose detections were also announced in Ackermann et al. (2017), are absent in the 4FGL/4LAC, possibly due to variability effects.

Figure 10 displays the photon index versus the gamma-ray luminosity for the different blazar classes. The trend of softer spectra with higher luminosity observed in earlier catalogs is confirmed. We reiterate the word of caution expressed in 3LAC: this trend is only significant when considering the whole sample of 4LAC blazars. It is not significant when considering the different blazar classes/subclasses individually. Figure 11 shows the corresponding plot for the nonblazar sources. Radio galaxies show a large scatter in photon index, while sources of the other classes have fairly soft spectra akin to those of FSRQs.

5.3. Variability

Variability is a key property of blazars and is known to depend on the energy band considered (e.g., Aleksić et al. 2015). This feature can be naturally explained as emitting electrons (assuming a leptonic scenario) of different energies, and thus different acceleration/cooling times contribute preferentially to the distinct bands. The assessment of variability in 4FGL does not only depend on intrinsic variability, but also on the overall significance of the source detection. Two different values of the variability index[79] are provided in 4FGL, derived from the sets of 1 yr and 2 month light curves. The 1 yr light curves allow the variability of fainter sources to be established compared to the monthly light curves used in early FGL catalogs. Because the variability indices are distributed as χ^2 functions with $N_{\rm dof}$ degrees of freedom, a source is defined as variable if at least one of the variability indices is greater than the 99% confidence limit of 18.48 and 72.44 for the 1 yr ($N_{\rm dof} = 7$) and 2 month ($N_{\rm dof} = 47$) light curves, respectively.

Figure 12 displays the TS distributions of variable sources compared to those of the whole sets of FSRQs and BL Lacs. All bright blazars are found to be variable. The fraction of variable sources goes down from 79% (464/591) for FSRQs to 35% for BL Lacs (362/1027). A monotonic trend is observed for the BL Lac subclasses, with fractions of 49% (140/288), 36% (98/270), and 31% (98/316) for LSPs, ISPs, and HSPs, respectively. Only 17% (157/941) of the BCUs show variability, as expected from the fact that these sources tend to be fainter (Section 5.1). The median fractional variability amplitude is 0.63 for FSRQs and 0.27 for BL Lacs. More extended studies about variability of the LAT-detected blazars can be found in the 3LAC paper.

Among the radio galaxies, IC 310, NGC 1275, 3C 120, NCG 1218, 3C 111, NGC 2892, and IC 4516 are found to be variable, hinting at a blazar-like behavior for these sources. All NLSy1s show significant variability, except for IERS B1303+515, B3 1441+476, TXS 2116−077. Three out of five CSS sources are variable (3C 138, 3C 309.1, 3C 380), as well as one SSRQ (3C 207). The three variable sources of the AGN class are: PKS 0521−36, PMN J1118−0413, and CGCG 050−083.

5.4. Potential Transiently Detected AGNs Missing in 4LAC

Some *Fermi*-LAT sources show blazar-like flaring activity during limited time intervals but do not meet the detection significance criterion to be included in the 4FGL, which is based on a summed 8 yr data set. We present here information about some of these transient sources spatially consistent with AGNs.

When undergoing periods of enhanced activity in 6 hr and 1 day time intervals, some sources can be caught in near-real time by the *Fermi*-LAT Flare Advocate Gamma-ray Sky Watcher (FAGSW) service (Ciprini & Fermi-LAT Collaboration 2012;

[79] The variability index is defined as twice the sum of the log(Likelihood) difference between the flux fitted in each time interval and the average flux over the full catalog interval.

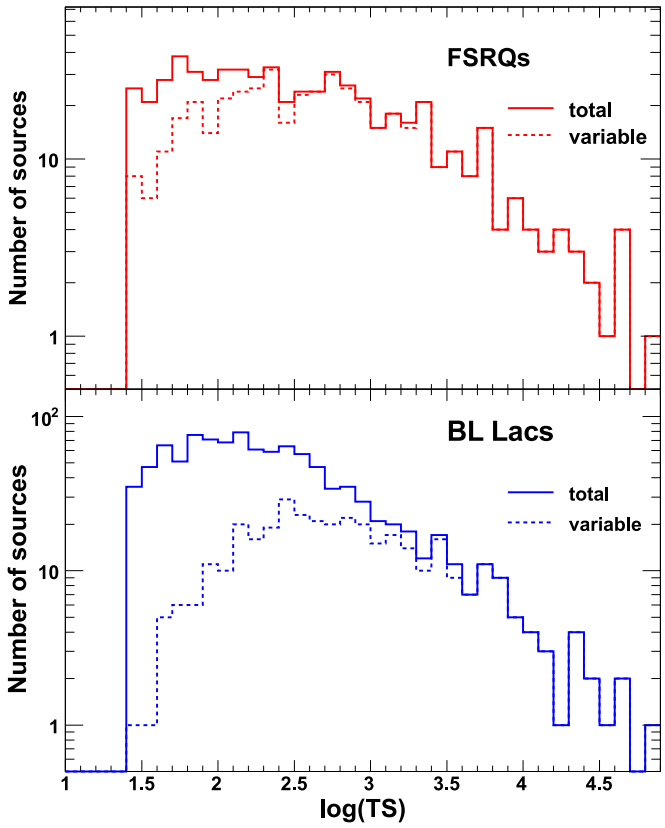

Figure 12. TS distributions of FSRQs (top) and BL Lacs (bottom) for variable sources and the whole sample.

Thompson et al. 2015, and references therein). The brightest sources are often reported to the community in Astronomer's Telegrams (ATels). A total of 371 ATels (plus three errata) were posted on behalf of the LAT Collaboration in the 8 yr period considered in the 4FGL/4LAC (2008 August 4 to 2016 August 2), and a total of 472 ATels were published from 2008 July 24 (ATel 1628) to 2019 August 15 (ATel 13032). At the time of writing, announced transient sources that were positionally consistent with blazars or other AGNs include: NVSS J104516 +275136 (ATel 12906); S5 0532+82 (ATel 12902; PKS 2247 −131 (ATels 9285, 9620, 11141); PKS 1915−458 ($z = 2.47$, ATels 2666, 2679, and already reported as missing in the 3FGL/3LAC catalogs); TXS 0135+291 (ATel 12888); 2MASX J15441967−0649156 ($z \simeq 0.04$, ATel 10482); PKS 1251−71 (ATel 8215), PMN J0508−5628 (ATel 6658); PMN J2010−2524 ($z = 0.825$, ATel 6553); TXS 1731+152A (ATel 6395, 6410); PKS 2136−642 (ATel 5695); and PKS 1510 −319 ($z = 1.71$, ATel 2528).

Sources detected on a one-week timescale were reported in the Second *Fermi*-LAT All-sky Variability Analysis (FAVA) Catalog (2FAV, Abdollahi et al. 2017), based on the first 7.4 yr of *Fermi*-LAT mission data. In the FAVA catalog,[80] the analysis was run in 100–800 MeV and 0.8–300 GeV energy bands, leading to the identification of 518 flaring gamma-ray sources. Among these sources, 13 were associated with established blazars or blazar candidates that are included in neither 4LAC nor 3LAC: PMN J0231−4746, 2MASS J06164292−4021527, TXS 0723+220, 4C +38.28 (B2 0913 +39), PKS 1200−051, PMN J1322−8419, PKS 1354−17, RX J1410.5+6100, PKS 1510−319, TXS 1534+378, TXS 1731 +152A, PKS 1824−582, 1RXS J235018.0−055928.

[80] https://fermi.gsfc.nasa.gov/ssc/data/access/lat/FAVA/

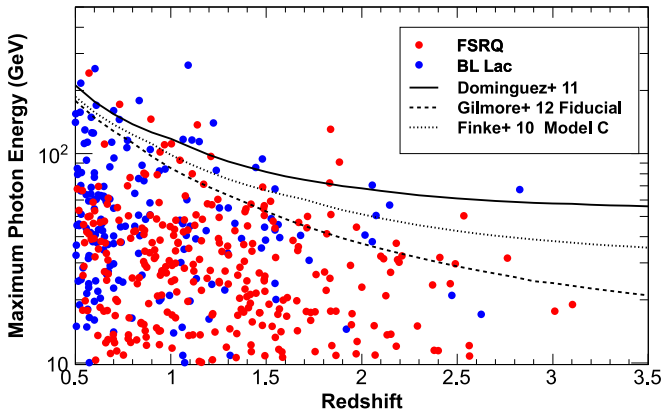

Figure 13. Energy of the highest-energy photon vs. redshift. Curves display the energies corresponding to an optical depth of 1 as predicted by different models.

For longer timescales, the first catalog of gamma-ray transient sources (1FLT, The Fermi LAT Collaboration in preparation) reports detections on monthly time intervals during the first 96 months of *Fermi*-LAT operation. This catalog contains 64 new gamma-ray sources not present in 4LAC/4FGL or earlier LAT catalogs. Their mean photon spectral index Γ of 2.6 indicates softer spectra than exhibited by the 4LAC sources (mean $\Gamma \sim 2.2$). These new sources include 24 BCUs (e.g., PKS 1649−031, TXS 0209+168, TXS 1601+160, PKS 2108−326 and others), 20 FSRQs (e.g., PKS 1524−13, TXS 1226+046, PKS 1200−051, PMN J2010 −2524, PKS 1706+006 and others), one BL Lac object (1RXS J112100.6+014515), one NLSy1 (Mkn 1501), and two radio galaxies (S5 1733+71 and PKS 2236−364).

5.5. Highest-energy Photons

The highest-energy photons detected for each source were selected within the purest—i.e., with the lowest instrumental background—class (P8R3_ULTRACLEANVETO_V2). Based on the energy-dependent PSF, we required a probability[81] greater than 0.95 for the photons to belong to the source being considered. Blazar gamma-ray spectra provide insight into the density of the EBL via the effect of photon-photon absorption, often defined in terms of an optical depth $\tau = 1$, where a photon has only a $1/e$ probability of reaching the observer (e.g., Abdollahi et al. 2018). A comparison between the energy of the highest-energy photon measured for a given source with the energy computed for $\tau = 1$ at that redshift by theoretical models of the EBL provides a simple and direct test of these models. Figure 13 compares the 4LAC highest-energy photons with the optical depth predictions of Finke et al. (2010), Domínguez et al. (2011), and Gilmore et al. (2012). Only a few photons exceed the $\tau = 1$ mark, thus remaining compatible with the predictions of these models.

[81] This probability is derived via the source-to-background ratio defined in appendix A of the 1FGL paper (Abdo et al. 2010b) and implemented in the adaptive-binning package available at https://fermi.gsfc.nasa.gov/ssc/data/analysis/user/.

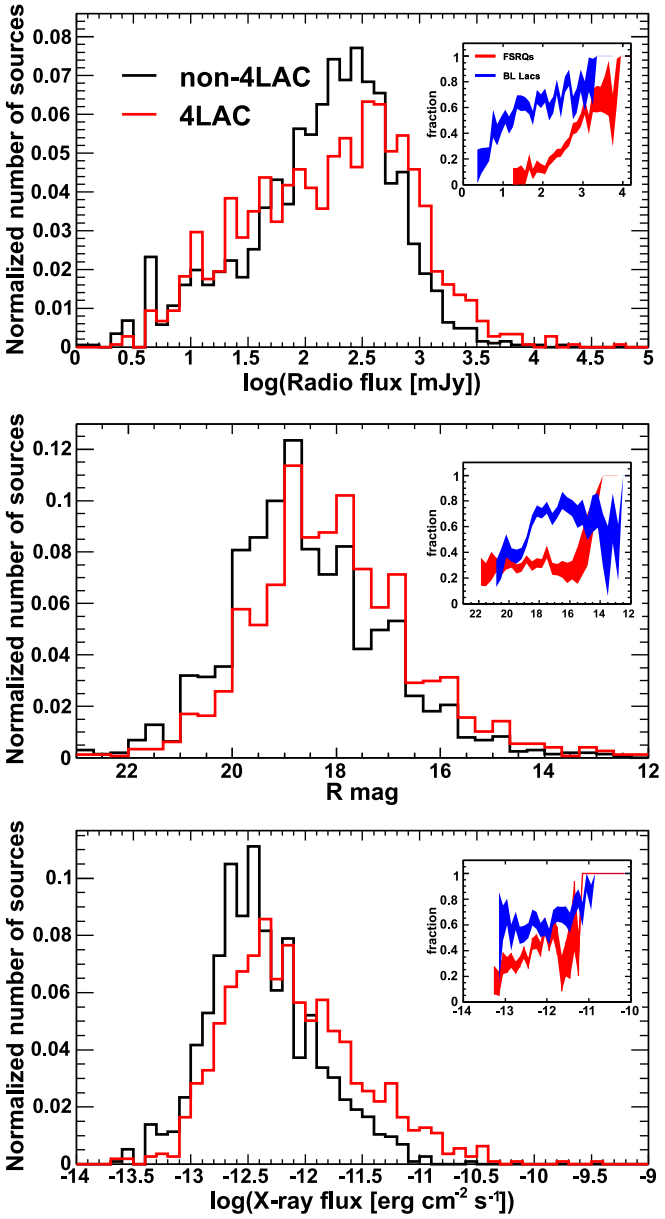

Figure 14. From top to bottom: radio flux density at 1.4 GHz, optical R magnitude, X-ray flux (0.1–2.4 keV) distributions for 4LAC (red) and non-4LAC (black) BZCAT sources. Insets show the fraction of 4LAC sources relative to the total for a given flux. Error bars have been omitted for clarity.

5.6. Gamma-Ray-detected versus Nondetected Blazars

The blazars detected in gamma-rays after 8 yr of LAT operation represent a sizable fraction of the whole population of known blazars as listed in BZCAT. This catalog represents an exhaustive list of all sources ever classified as blazars, but is by no means complete. Although a comparison between the gamma-ray-detected and nondetected blazars within that sample has no strong statistical meaning in terms of relative weights, it is nevertheless useful to look for general trends.

In total, the 4LAC includes 29% (562/1909), 66% (764/1151), and 38% (88/227) of the BZCAT (Massaro et al. 2015) FSRQs, BL Lacs, and BCUs, respectively. Out of the 1353 new 4FGL sources, 405 are present in BZCAT. Figure 14 compares the distributions of radio flux at 1.4 GHz, optical *R*-band magnitude, and X-ray (0.1–2.4 keV) fluxes for the gamma-ray-detected and nondetected BZCAT blazars, as well as the fraction of gamma-ray-detected blazars relative to the total as a function of the different fluxes. The gamma-ray-detected blazars are somewhat brighter on average in all bands, confirming previous findings (Lister et al. 2011; Böck et al. 2016; Paliya et al. 2017). The fraction of 4LAC blazars in the total population of BZCAT blazars remains non-negligible even at the faint ends of the radio, optical, and X-ray flux distributions, in particular for BL Lacs. This observation is a clue that even the faintest known blazars could eventually shine in gamma-rays at LAT-detection levels.

5.7. Sources Detected at Very High Energies

Table 7 shows the list of 78 AGNs detected by ground-based Cerenkov telescopes, as listed in TeVCat.[82] All are present in 4LAC, and the table shows their optical and SED-based classes, redshifts, and 4LAC photon indices. The 3LAC catalog included 55 of the 56 VHE AGNs with detections published or announced at that time; only HESS J1943+213 was missing. The overall mean of the 4LAC photon indices for these VHE AGNs is 1.91 ± 0.20. For the most numerous subclass, the HSP BL Lacs, we find the mean index to be 1.81 ± 0.08, i.e., a very hard gamma-ray spectrum. Of the 78, 56 4LAC AGNs are variable at a significance greater than 99%.

5.8. Miscellaneous Notes About Individual Sources

In the course of the 4LAC analysis, we found a number of individual sources that have changed classification or have unclear associations. We include this information about them for completeness. In case of conflicting associations, we only retained the most probable one in the 4LAC catalog.

1. 4FGL J0140.6−0758 is associated with the BL Lac RX J0140.7−0758. Another object, SDSS J014040.63 −075857.2, is located 9″ away (i.e., $0.04r_{95}$, where r_{95} is the 95% confidence radius), at a redshift of 2.674 coming from a broad-line SDSS optical spectrum. This source has no reported radio emission.
2. 4FGL J0242.3+5216 has two possible high-confidence associations: with GB6 J0242+5209 and TXS 0239 +520, which have similar brightness in the radio band.
3. 4FGL J0337.8−1157 is associated with PKS 0335−122, a distant FSRQ at $z = 3.442$ that has a damped Lyα absorption system at $z = 3.180$ along the line of sight (Kanekar & Chengalur 2003).
4. 4FGL J0618.1+7819 is associated with the starburst galaxy NGC 2146 ($z = 0.002975$), but the FSRQ 6C 060948+781625 ($z = 1.43$) has a similar association probability.
5. 4FGL J0647.7−4418 is associated with the high-mass X-ray binary RX J0648.0−4418 in 4FGL, but the blazar candidate SUMSS J064744−441946 has a just barely lower association probability (0.80 versus 0.85).
6. 4FGL J0720.0−6237 is associated with the FSRQ PMN J0716−6240, but another FSRQ, PMN J0719−6218, lies just outside the 95% confidence region and might contribute to the gamma-ray emission.
7. 4FGL J0814.4+2941 is associated with the BL Lac EXO 0811.2+2949, but a broad-line quasar, SDSS J081425.89 +294115.6, also lies within the 95% confidence region.

[82] http://tevcat.uchicago.edu/, as of 2019 March.

Table 7
Properties of the 4LAC VHE AGNs

4FGL Name	Name	Source Class	SED Type	Redshift	Photon Index	Variability Index[a]
J0013.9-1854	RBS 0030	bll	HSP	0.09	1.97 ± 0.1	2.61
J0033.5-1921	KUV 00311-1938	bll	HSP	0.61	1.77 ± 0.02	27.17
J0035.9+5950	1ES 0033+595[b]	bll	HSP	⋯	1.75 ± 0.02	149.76
J0112.1+2245	S2 0109+22	bll	LSP	0.26	2.07 ± 0.01	313.15
J0136.5+3906	B3 0133+388	bll	HSP	⋯	1.71 ± 0.02	51.08
J0152.6+0147	PMN J0152+0146	bll	HSP	0.08	1.96 ± 0.06	15.23
J0214.3+5145	TXS 0210+515[b]	bll	HSP	0.05	1.88 ± 0.09	11.2
J0221.1+3556	B2 0218+357	fsrq	LSP	0.94	2.29 ± 0.01	3327.03
J0222.6+4302	3C 66A	bll	ISP	0.44	1.96 ± 0.01	976.11
J0232.8+2018	1ES 0229+200	bll	HSP	0.14	1.78 ± 0.11	4.36
J0238.4-3116	1RXS J023832.6-311658	bll	HSP	0.23	1.8 ± 0.04	33.44
J0303.4-2407	PKS 0301-243	bll	HSP	0.27	1.9 ± 0.02	253.95
J0316.8+4120	IC 310	rdg	ISP	0.02	1.78 ± 0.18	19.86
J0319.8+4130	NGC 1275	rdg	LSP	0.02	2.12 ± 0.01	1970.98
J0319.8+1845	1E 0317.0+1835	bll	HSP	0.19	1.67 ± 0.07	32.33
J0349.4-1159	1ES 0347-121	bll	HSP	0.19	1.76 ± 0.1	10.0
J0416.9+0105	1ES 0414+009	bll	HSP	0.29	1.89 ± 0.07	9.76
J0449.4-4350	PKS 0447-439	bll	HSP	0.2	1.85 ± 0.01	55.2
J0507.9+6737	1ES 0502+675	bll	HSP	0.42	1.58 ± 0.03	39.18
J0509.4+0542	TXS 0506+056	bll	ISP	0.34	2.08 ± 0.02	245.91
J0521.7+2112	TXS 0518+211[b]	bll	HSP	0.11	1.92 ± 0.01	682.16
J0550.5-3216	PKS 0548-322	bll	HSP	0.07	1.89 ± 0.1	5.98
J0627.0-3529	PKS 0625-35	rdg	HSP	0.05	1.9 ± 0.04	11.56
J0648.7+1516	RX J0648.7+1516[b]	bll	HSP	0.18	1.7 ± 0.04	3.2
J0650.7+2503	1ES 0647+250	bll	HSP	0.2	1.74 ± 0.02	117.43
J0710.4+5908	1H 0658+595	bll	HSP	0.13	1.68 ± 0.05	26.55
J0721.9+7120	S5 0716+71	bll	ISP	0.13	2.06 ± 0.01	1554.68
J0733.4+5152	NVSS J073326+515355	bcu	HSP	0.06	1.8 ± 0.1	14.97
J0739.2+0137	PKS 0736+01	fsrq	LSP	0.19	2.41 ± 0.02	1983.59
J0809.8+5218	1ES 0806+524	bll	HSP	0.14	1.88 ± 0.02	290.4
J0847.2+1134	RX J0847.1+1133	bll	ISP	0.2	1.72 ± 0.08	8.47
J0854.8+2006	OJ 287	bll	LSP	0.31	2.23 ± 0.01	611.67
J0958.7+6534	S4 0954+65	bll	LSP	0.37	2.21 ± 0.02	2012.73
J1010.2-3119	1RXS J101015.9-311909	bll	HSP	0.14	1.75 ± 0.07	34.16
J1015.0+4926	1H 1013+498	bll	HSP	0.21	1.84 ± 0.01	195.6
J1103.6-2329	1ES 1101-232	bll	HSP	0.19	1.73 ± 0.08	10.7
J1104.4+3812	Mkn 421	bll	HSP	0.03	1.78 ± 0.01	1028.05
J1136.4+6736	RX J1136.5+6737	bll	HSP	0.14	1.75 ± 0.05	23.5
J1136.4+7009	Mkn 180	bll	HSP	0.05	1.8 ± 0.03	20.39
J1144.9+1937	3C 264	rdg	HSP	0.02	1.94 ± 0.1	4.15
J1159.5+2914	Ton 599	fsrq	LSP	0.73	2.26 ± 0.01	1391.63
J1217.9+3007	B2 1215+30	bll	HSP	0.13	1.95 ± 0.01	396.98
J1221.3+3010	PG 1218+304	bll	HSP	0.18	1.71 ± 0.02	44.28
J1221.5+2814	W Comae	bll	ISP	0.1	2.16 ± 0.02	243.32
J1224.4+2436	MS 1221.8+2452	bll	HSP	0.22	1.89 ± 0.04	148.48
J1224.9+2122	4C +21.35	fsrq	LSP	0.43	2.33 ± 0.01	17566.6
J1230.2+2517	ON 246	bll	ISP	0.14	2.09 ± 0.02	1651.75
J1230.8+1223	M87	rdg	ISP	0.01	2.06 ± 0.04	16.98
J1256.1-0547	3C 279	fsrq	LSP	0.54	2.34 ± 0.01	5667.24
J1315.0-4236	MS 13121-4221	bll	HSP	0.1	1.72 ± 0.1	6.61
J1325.5-4300	Cen A	rdg	LSP	0.01	2.65 ± 0.02	8.25
J1427.0+2348	PKS 1424+240	bll	HSP	0.6	1.82 ± 0.01	205.42
J1428.5+4240	H 1426+428	bll	HSP	0.13	1.66 ± 0.05	14.91
J1442.7+1200	1ES 1440+122	bll	HSP	0.16	1.8 ± 0.07	10.06
J1443.9-3908	PKS 1440-389	bll	HSP	0.07	1.82 ± 0.02	22.05
J1443.9+2501	PKS 1441+25	fsrq	LSP	0.94	2.08 ± 0.02	2858.38
J1512.8-0906	PKS 1510-089	fsrq	LSP	0.36	2.38 ± 0.01	4421.04
J1517.7-2422	AP Librae	bll	LSP	0.05	2.12 ± 0.02	90.89
J1518.0-2731	TXS 1515-273	bll	HSP	⋯	2.06 ± 0.05	57.84
J1555.7+1111	PG 1553+113	bll	HSP	0.36	1.68 ± 0.01	74.97
J1653.8+3945	Mkn 501	bll	HSP	0.03	1.75 ± 0.01	292.85
J1725.0+1152	1H 1720+117	bll	HSP	0.18	1.86 ± 0.02	13.33
J1728.3+5013	I Zw 187	bll	HSP	0.05	1.78 ± 0.03	164.28

Table 7
(Continued)

4FGL Name	Name	Source Class	SED Type	Redshift	Photon Index	Variability Index[a]
J1744.0+1935	S3 1741+19	bll	HSP	0.08	1.93 ± 0.05	10.72
J1751.5+0938	OT 081	bll	LSP	0.32	2.26 ± 0.02	884.58
J1944.0+2117	MG2 J194359+2118[b]	bcu		⋯	1.53 ± 0.09	15.42
J2000.0+6508	1ES 1959+650	bll	HSP	0.05	1.82 ± 0.01	1052.41
J2001.2+4353	MG4 J200112+4352[b]	bll	HSP	⋯	1.95 ± 0.02	1027.21
J2009.4-4849	PKS 2005-489	bll	HSP	0.07	1.83 ± 0.02	135.08
J2039.5+5218	1ES 2037+521[b]	bll	HSP	0.05	1.88 ± 0.09	4.58
J2056.7+4939	RGB J2056+496[b]	bcu	HSP	⋯	1.85 ± 0.04	23.86
J2158.8-3013	PKS 2155-304	bll	HSP	0.12	1.85 ± 0.01	646.95
J2202.7+4216	BL Lac	bll	LSP	0.07	2.23 ± 0.01	2474.03
J2243.9+2021	RGB J2243+203	bll	HSP	⋯	1.86 ± 0.02	116.39
J2250.0+3825	B3 2247+381	bll	HSP	0.12	1.72 ± 0.06	24.53
J2324.7-4041	1ES 2322-409	bll	HSP	0.17	1.78 ± 0.05	49.44
J2347.0+5141	1ES 2344+514[b]	bll	HSP	0.04	1.81 ± 0.02	56.97
J2359.0-3038	H 2356-309	bll	HSP	0.17	1.93 ± 0.07	1.77

Notes.
[a] A variability index greater than 18.47 indicates that the source is variable at a significance greater than 99%.
[b] Refers to low-latitude sources (not in 4LAC).

(This table is available in machine-readable form.)

8. 4FGL J0941.9+2724 may have a double association with the BL Lac 5BZBJ0941+2722 and the FSRQ MG2 J094148+2728, which was an association in 3FGL.
9. 4FGL J1300.4+1416 (3FGL J1300.2+1416) is associated with OW 197 (PKS 1257+145, $z = 1.1085$), as it was in 3LAC. At about 5′ distance from OW 197, a blazar candidate NVSS J130041+141728 lies in both the 3FGL and 4FGL 95% confidence ellipses, despite a reduction in size of the ellipse by a factor of 4. The 4FGL source position is about midway between OW 197 and NVSS J130041+141728.
10. 4FGL J1625.7+4134 may have a double association, with 4C +41.32 and B3 1624+414.

6. Summary

The 4LAC, derived from the 4FGL catalog, based on 8 yr of *Fermi*-LAT data, includes 1353 (85%) more AGNs than the 3LAC. At high Galactic latitudes, AGNs represent at least 79% of the 4FGL sources. Unassociated sources lying in this sky region share common spectral features with BCUs (see Figure 22 of the 4FGL paper), suggesting that most of them are AGNs as well. BL Lacs and FSRQs represent 38% and 24% of the blazar population, respectively. The increase of the fraction of BCUs in the sample from 29% in 3LAC to 38% in 4LAC emphasizes the value of the spectroscopic endeavor carried out by several groups. From their photon index and $\nu_{\rm s,peak}$ distributions, BCUs probably contain similar fractions of (still unclassified) FSRQs and BL Lacs as observed in the classified population.

Fits of the synchrotron-peak positions have been performed manually for all 4LAC sources, leading to an SED-based classification for 75% of the 4LAC blazars. The number of nonblazar AGNs has almost doubled relative to 3LAC, from 32 to 64, including 22 new radio galaxies. The overall properties of the 4LAC AGNs are similar to those found in 3LAC. A fairly clear separation in spectral hardness between BL Lacs and FSRQs is observed, with a transition around $\Gamma = 2.25$. Five HSP FSRQs, which do not fit with the "blazar sequence" picture, are present in 4LAC. They all show spectra harder than average for the FSRQ class. Significant spectral curvature is observed for essentially all the brightest (TS > 3000) blazars. The redshift distributions of newly detected blazars resemble those found for 3LAC. Five new FSRQs have redshifts greater than the highest 3LAC redshift ($z = 3.1$), reaching $z = 4.31$. The correlation between photon index and gamma-ray luminosity is strong overall for blazars, but much weaker if the different classes are taken separately. Analysis of 1 yr and 2 month light curves shows that 79% of the FSRQs and 35% of the BL Lacs are variable, along with seven radio galaxies and 16 other AGNs. The highest-energy photons show compatibility with the EBL γ–γ attenuation predicted by some recent models. About 30% of the new blazars are present in BZCAT. Although the 4LAC blazars are predominantly associated with higher-than-average radio, optical, and X-ray fluxes in BZCAT, they remain non-negligible even at the faint ends of these flux distributions, in particular for BL Lacs. All 78 known VHE blazars are detected by the LAT, with 56 of them being variable in the GeV range.

The *Fermi* LAT Collaboration acknowledges generous ongoing support from a number of agencies and institutes that have supported both the development and the operation of the LAT as well as scientific data analysis. These include: the National Aeronautics and Space Administration and the Department of Energy in the United States; the Commissariat à l'Energie Atomique and the Centre National de la Recherche Scientifique/Institut National de Physique Nucléaire et de Physique des Particules in France; the Agenzia Spaziale Italiana and the Istituto Nazionale di Fisica Nucleare in Italy; the Ministry of Education, Culture, Sports, Science, and Technology (MEXT), High Energy Accelerator Research Organization (KEK), and Japan Aerospace Exploration Agency (JAXA) in Japan; and the K. A. Wallenberg Foundation, the Swedish Research Council, and the Swedish National Space Board in Sweden. Additional support for science analysis

during the operations phase is gratefully acknowledged from the Istituto Nazionale di Astrofisica in Italy and the Centre National d'Études Spatiales in France. This work was performed in part under DOE Contract DE- AC02-76SF00515.

This research has made use of data obtained from the high-energy Astrophysics Science Archive Research Center (HEASARC) provided by NASA's Goddard Space Flight Center; the SIMBAD database operated at CDS, Strasbourg, France; and the NASA/IPAC Extragalactic Database (NED) operated by the Jet Propulsion Laboratory, California Institute of Technology, under contract with the National Aeronautics and Space Administration. This research has made use of data archives, catalogs and software tools from the ASDC, a facility managed by the Italian Space Agency (ASI). Part of this work is based on the NVSS (NRAO VLA Sky Survey). The National Radio Astronomy Observatory is operated by Associated Universities, Inc., under contract with the National Science Foundation. This publication makes use of data products from the Two Micron All Sky Survey, which is a joint project of the University of Massachusetts and the Infrared Processing and Analysis Center/California Institute of Technology, funded by the National Aeronautics and Space Administration and the National Science Foundation. This publication makes use of data products from the *Wide-field Infrared Survey Explorer*, which is a joint project of the University of California, Los Angeles, and the Jet Propulsion Laboratory/California Institute of Technology, funded by the National Aeronautics and Space Administration. Funding for the SDSS and SDSS-II has been provided by the Alfred P. Sloan Foundation, the Participating Institutions, the National Science Foundation, the U.S. Department of Energy, the National Aeronautics and Space Administration, the Japanese Monbukagakusho, the Max Planck Society, and the Higher Education Funding Council for England. The SDSS Web Site is http://www.sdss.org/. The SDSS is managed by the Astrophysical Research Consortium for the Participating Institutions. The Participating Institutions are the American Museum of Natural History, Astrophysical Institute Potsdam, University of Basel, University of Cambridge, Case Western Reserve University, University of Chicago, Drexel University, Fermilab, the Institute for Advanced Study, the Japan Participation Group, Johns Hopkins University, the Joint Institute for Nuclear Astrophysics, the Kavli Institute for Particle Astrophysics and Cosmology, the Korean Scientist Group, the Chinese Academy of Sciences (LAMOST), Los Alamos National Laboratory, the Max-Planck-Institute for Astronomy (MPIA), the Max-Planck-Institute for Astrophysics (MPA), New Mexico State University, Ohio State University, University of Pittsburgh, University of Portsmouth, Princeton University, the United States Naval Observatory, and the University of Washington.

Appendix
Chronological Convention for Source Association Naming

In 3LAC and 4LAC, an approximate chronological scheme is adopted for the proper names of the radio/IR/optical/X-ray counterparts. For greater convenience and clarity, a time-ordered list of the source catalogs used here is given in Table 8. The proper names follow approximately the initial (discovery) names from radio, IR, optical, and X-ray surveys, catalogs and observations. These names have been checked to be recognized by the strict "name resolver" in the NASA-IPAC Extragalactic Database (and therefore by many other web databases like HEASARC derived from it).

Radio galaxies, quasars, blazars, and other AGNs were first discovered as optical non-starlike nebulae objects (i.e., galaxies) listed in the C. Messier catalog in year 1791, and the NGC (J.L.E. Dreyer) and IC catalogs published between the years 1781 and 1905. Examples of sources in 4LAC are the radio galaxies M87, NGC 315, NGC 1275 (also known as Per A or 3C 84), and the starburst galaxies M82, NGC 253, and NGC 1068. Other AGNs were initially considered as optical variable stars (Argelander, e.g., BL Lac, W Com, AP Lib, and BW Tau, known as 3C 120). Some blazars and AGNs were discovered as unusual optically blue starlike objects (Ton, PHL, Mkn catalogs, about 1957–1974; for example, Ton 599, Mkn 180, Mkn 421, Mkn 501, PHL 1389) or in optical galaxy catalogs (CGCG, MCG, CGPG, ARP, UGC, Ark, Zw/I-V, Tol, during the period 1961–1976; for example, CGCG 050-083, UGC 773, I Zw 187, V Zw 326). Subsequent optically selected objects and quasar catalogs provide some names of 4LAC associations (for example, PG, PB, US, SBS, PGC, LEDA, HS, SDSS).

In parallel, the largest fraction of radio galaxies and AGNs were discovered during the early era of radio astronomy, with objects like Vir A, Cen A, Cen B, Per A appearing already in the first half of the 1950s, and the well-known point radio source catalogs 3C, CTA, PKS, 4C, O[+letter], VRO, NRAO, AO, DA, B2, GC, and S1/S2/S3 all published between about 1959 and 1974. The PKS (Parkes Radio Catalog, Australia) is the source name preferred for southern celestial radio AGNs, while northern radio AGNs were likely first reported in Cambridge catalogs (especially 3C, 4C) and the Ohio State University Radio Survey Catalog (Ohio Big Ear radio-antenna, O(x) catalog prefix), or in the CTA, NRAO, DA, B2, TXS, S1-5, or MG1-4 catalogs. Examples in the 4LAC are Cen A (already known as NGC 5128, but better known with its original radio name), Per A, Vir A (M87). Other radio catalogs published between about 1974 and the mid-1980s are include TXS, 5C, S4/S5, MRC, and B3, while from the end of the 1980s until the end of 1990s, we have MG1/MG2/MG4, 87 GB, 6C/7C, JVAS, PMN, EF, CJ2, FIRST, Cul, GB6, FBQS, WN, NVSS, CLASS, IERS, SUMSS, and CRATES. Some catalogs at IR or UV frequencies are also considered here (KUV, *EUVE*, 2MASSi, 2MASS). Further blazars and other AGNs, fainter in the radio band, were discovered directly thanks to the observations made by the first X-ray satellites (2A, 4U, XRS, EXO, H/1H, MS, 1E, 1ES, 2E, RX catalogs published from about 1978 to the mid-1990s). Later came the *ROSAT* survey catalogs from reanalysis and cross-matches, such as RGB, RBS, RHS, 1RXS, XSS.

Table 8 reports catalog and survey prefixes in an approximate chronological order that was adopted for the association names of the 4LAC catalog. The order is only approximate, due to the lack of precise information for each catalog as well as the need to follow, in some cases, the criterion of the most-used name in the literature and published papers for a source (even if this latter choice is rather arbitrary and subject to opinion).

The most frequent source association names in 4LAC come from the 3C, 4C, PKS, O[+letter], B2, S2/S3/S5, TXS, MG1/MG2, PMN, GB6, SDSS, 1ES, RX, RBS, 1RXS, NVSS, and 2MASS catalogs. Some 4LAC counterpart proper names may be somewhat inadequate because of the radio extension of the

Table 8
Historical Catalogs Reference for Naming of 4LAC Associations

Waveband	Publ. Year(s)/Range	Prefix	Catalog Name
Optical	1781	M	Charles Messier catalog of nebulae and non-starlike objects from M1 to M110.
Optical	1844–∼1915	xy+const.	Argelander convention for first-discovered variable stars in each constellations.
Optical	1848	GC	General Catalog
Optical	1888	NGC	New General Catalog
Optical	1896, 1905	IC	IC Index Catalogs (IC I and IC II, expansions of the NGC Catalog).
Radio	1947-1949	const.+letter	Constellation + Arabic letter (first radio sources ever discovered).
Optical	1952, 1963	PLX	Yale General Catalog of Trigonometric Stellar Parallaxes
Radio	1955	2C	Second Cambridge Radio Catalog at 178 MHz
Optical	1957–1959	Ton	Tonantzintla (Mexico) Catalog of Blue Stars
Radio	1959–1962	3C	Third Cambridge Radio Catalog at 178 MHz (3C, 3CR)
Radio	1960	CTA	Caltech Radio Survey List A
Optical	1961–1968	CGCG	Catalog of Galaxies and of Clusters of Galaxies
Optical	1962	PHL	Palomar-Haro-Luyten Blue Stellar Objects list
Optical	1962–1974	MCG	Morphological Catalog of Galaxies
Radio	1964–1967	Kes	Kesteven catalog of galactic radio sources
Radio	1964–1968, 1971–1975	PKS	Parkes catalog of radio sources
Radio	1965–1969	4C	Fourth Cambridge Radio Catalog
Radio	1965–1971	O(x) (Ohio (x))	Big Ear Ohio State University Radio Survey Catalog (O + R.A.hour letter)
Radio	1965–1971	VRO	Vermillion Radio Observatory survey catalog
Radio	1966	NRAO	National Radio Astron. Obs. Positions and Flux Densities of Radio Sources
Optical	1966	ARP	Arp Peculiar Galaxies catalog
Radio	1967–1970	AO	Arecibo Occultation Radio Sources
Optical	1967–1974	Mkn (Mrk)	Markaryan blue object list (Galaxies with an ultraviolet continuum)
Radio	1968	DA	Dominion Radio Observatory Survey, List A
Radio	1970–1974	B2	Second Bologna Catalog of radio sources
Radio	1971–1972	GC	Green Bank Radio Survey List C
Radio	1971–1972	S1/S2/S3	First/Second/Third "Strong" (radio) Source survey
Radio	1971–1972	GB (GB1)	Green Bank Radio Survey
Radio	1971–1978	GB2	Green Bank Radio Survey 2
Optical	1971	CGPG	Catalog of Selected Compact Galaxies and of Post-Eruptive Galaxies
Optical	1973	UGC	Uppsala General Catalog of Galaxies
Radio	1974–1983	TXS	Texas Survey of Radio Sources
Optical	1974	UGCA	Uppsala General Catalog Appendix
Radio	1975	5C	Fifth Cambridge Survey of Radio Sources
Optical	1975	Ark	Arakelian Emission Line Objects
Optical	1975	I-V Zw	First/Second/Third/Fourth/Fifth Zwicky list of compact galaxies
Optical	1976	Tol	Tololo List of Emission Line Galaxies
Optical	1976, 1983, 1986	PG	Palomar-Green Bright Quasar Catalog
Optical	1977–1984	PB	Palomar-Berger Faint Blue Stars Catalog
Radio	1978	S4	Fourth "Strong" (radio) Source survey
X-ray	1978	2A	Second ARIEL V survey catalog
X-ray	1978	4U	Fourth Uhuru Catalog of X-ray Sources
Radio	1978–1995	GRA (GR)	Grakovo Radio Decametric Survey
X-ray	1979	XRS	X-Ray Source catalog from rockets, balloons, satellites of 1964–1977
Ultraviolet	1980–1984	KUV	KisoUltraviolet Excess Objects catalogs
Optical	1980–1993	USNO (IDS)	U.S. Naval Observatory parallaxes catalog
Radio	1981	S5	Fifth "Strong" (radio) Source survey
X-ray	1981	3A	Third ARIEL V survey catalog
Gamma-ray	1981	2CG	Second COS-B catalog of high-energy gamma-ray sources
Optical	1981–1984	US	Usher Faint Blue Stars
Radio	1981, 1991	MRC	Molonglo Reference Catalog of Radio Sources
Radio	1981, 1994	1 Jy	Extragalactic radio sources with flux densities >1 Jy at 5 GHz catalog
Optical	1983–2000	SBS	Second Byurakan Survey of Emission Line Objects
X-ray	1983–1986	EXO	*EXOSAT* X-Ray Source Catalog
X-ray	1984	H (1H)	The *HEAO* A-1 X-Ray Source Catalog
X-ray	1984	EXO	*EXOSAT* XRay Source Catalog
Radio	1985	B3	Third Bologna Catalog of radio sources
Radio	1985–1993	6C	Sixth Cambridge Radio Catalog
Radio	1986	MG1	First MIT-Green Bank 5 GHz Survey
Optical	1987	AM	Arp and Madore Southern Peculiar Galaxies and Associations catalog
Infrared	1988	IRAS	Infrared Astronomy Satellite Point Source Catalog
Infrared	1990	IRAS F	Infrared Astronomy Satellite Faint Source Catalog
Optical	1989	PGC	Principal Galaxy Catalog

Table 8
(Continued)

Waveband	Publ. Year(s)/Range	Prefix	Catalog Name
Optical	1989	LEDA	Lyon-Meudon Extragalactic Database catalog
Optical	1989	[HB89]	Hewitt and Burbidge QSO compilation (mute prefix)
Optical	1989–1996	CTS	Calan-Tololo Survey of galaxies and quasars
Radio	1990	MG2	Second MIT-Green Bank 5 GHz Survey
Radio	1990	MG3	Third MIT-Green Bank 5 GHz Survey
Optical	1990	GSC	Hubble Guide Star Catalog
Radio	1990-1998	7C	Seventh Cambridge Survey of Radio Sources
X-ray	1990	1E	The Einstein Observatory (*HEAO* 2) catalog of IPC X-ray sources.
Radio	1991	MG4	Fourth MIT-Green Bank 5 GHz Survey
Radio	1991	87 GB	The 1987 Green Bank Radio Survey
Optical	1991–2007	HS (HE)	Hamburg/ESO QSO Survey
X-ray	1991	MS	Einstein (*HEAO*-2) Medium Sensitivity Survey
X-ray	1991	1ES	1st Einstein (*HEAO*-2) Slew Survey Source Catalog
Radio	1992	ZS	Zelenchuk Survey
Gamma-ray	1992–2000	GRO	Compton Gamma Ray Observatory source
Radio	1992–2002	JVAS	Jodrell Bank-VLA Astrometric Survey
Optical	1993	HIP	Hipparcos Catalog
Radio	1994	PMN	Parkes-MIT-NRAO Radio Survey catalog
Radio	1994	EF	Effelsberg Radio Sources catalog
Radio	1994	CJ2	Second Caltech-Jodrell Bank VLBI Survey catalog
Ultraviolet	1994	*EUVE*	Extreme UltraViolet Explorer Bright Source List
X-ray	1994	RX	First *ROSAT* Source Catalog of pointed observations with the PSPC
X-ray	1994	2E	Second Einstein (*HEAO*-2) Observatory catalog of IPC X-ray sources
Radio	1995–1997	FIRST	Faint Images of the Radio Sky at Twenty Centimeters
Radio	1995	Cul	Culgoora Radio Sources catalog
X-ray	1995	1WGA	First White Giommi Angelini *ROSAT* X-Ray sources list
Radio	1996	GB6	Green Bank 6 cm Radio Survey
Radio	1996	CJF	Caltech-Jodrell bank Flat spectrum survey
Ultraviolet	1996	2EUVE	2nd Extreme Ultraviolet Explorer source catalog
Radio	1996–2001	FBQS	FIRST Bright QSO Survey
Radio	1997, 2008	WN	WENSS North radio survey
X-ray	1997	RGB	*ROSAT*-Green Bank source catalog
X-ray	1997	EXSS	Einstein (*HEAO*-2) Extended X-Ray Sources
Radio	1998	NVSS	NRAO VLA Sky Survey
Radio	1998–2002	CLASS	Cosmic Lens All-Sky Survey catalog
Radio	1998–2010	IERS	International Earth Rotation Service
Radio	1998–2010	ICRF	International Celestial Reference Frame
Infrared	1998-2000	2MASSi	2 Micron All Sky Survey point sources Incremental release
X-ray	1998–2000	RBS	*ROSAT* Bright Survey catalog
X-ray	1998–2000	RHS	*ROSAT* Hard X-ray Spectra source catalog
Gamma-ray	1999	3EG	Third EGRET Catalog of High-Energy Gamma-Ray Sources
Optical	1999	MRSS	Muenster Red Sky Survey
Optical	1999–2008	SDSS	Sloan Digital Sky Survey Catalogs
X-ray	1999–2000, 2006, 2009	1RXS	*ROSAT* All-Sky Survey Bright Source Catalog
Radio	2000	VSOP	VLBI Space Observatory Programme
X-ray	2001, 2005	1AXG	1st ASCA X-ray survey from GIS experiment
Radio	2003, 2008	SUMSS	Sydney University Molonglo Sky Survey catalog
Radio	2003–2009	*WMAP*	*WMAP* Foreground Source Catalogs
Infrared	2003–2006	2MASS	2 Micron All Sky Survey Point objects Final Release
X-ray	2004	XSS	*RXTE* XTE Slew Survey catalog
X-ray	2004–2008	IGR	*INTEGRAL* Gamma Ray source
Ultraviolet	2005–2015	GALEXASC	GALaxy Evolution eXplorer All-Sky Survey Source Catalog
X-ray	2005	SHBL	Sedentary High energy peaked BL Lacs
X-ray	2005–2015	SWIFT	Swift source list
Gamma-ray	2006-...	HESS	High Energy Stereoscopic System observatory source list
Radio	2007	CRATES	Combined Radio All-Sky Targeted Eight GHz Survey
Radio	2007	VIPS	VLBA Imaging and Polarimetry Survey
Radio	2007	VERA	VLBI Exploration of Radio Astrometry
Radio	2007–2008	VLSS	VLA Low-frequency Sky Survey
X-ray	2007	SAXWFC	Beppo-SAX X-Ray Satellite Wide Field Camera catalog
X-ray	2007-2010	1XMM	1st *XMM-Newton* Serendipitous Source Catalog
X-ray	2007-2010	2XMM	2nd *XMM-Newton* Serendipitous Source Catalog
Radio	2008	CGRaBS	Candidate Gamma-Ray Blazar Survey

Table 8
(Continued)

Waveband	Publ. Year(s)/Range	Prefix	Catalog Name
Gamma-ray	2008	EGR	Revised catalog of gamma-ray sources detected by EGRET
Radio	2008–2010	AT20G	Australia Telescope 20 GHz Survey catalog
Gamma-ray	2008-...	VER	VERITAS gamma-ray source list
Gamma-ray	2009	1AGL	First AGILE GRID Catalog of High Confidence Gamma-Ray Sources
Multifrequency	2009–2018	BZ(x) (2-5BZ(x))	Roma Blazar catalog (the last published has prefix 5BZ+(letter))
Infrared	2010	*AKARI*-IRC-V1	*AKARI*/IRC Point Source Catalog Version 1
X-ray	2010	2PBC	Second Palermo *Swift*-BAT hard X-ray catalog
Infrared	2011	*WISE*	*Wide-field Infrared Survey Explorer* catalog
X-ray	2012	CXO	Chandra Source Catalog Release 1.1
Optical	2012, 2014	LQAC	Large Quasar Astrometric Catalog
Infrared	2013	SSTSL2	Spitzer Space Telescope Source List—version 4.2
X-ray	2013	2MAXI	Monitor of All-sky X-ray Image 37 month catalog
Millimeter	2013	PLCKERC0(nn)	Planck Early Release Compact Source Catalog at (nn)GHz
Radio	2014	WB (WIBRaLS)	*WISE* Blazar-like Radio-loud Sources
Ultraviolet	2016	UVQS	UV-bright Quasar Survey
Radio	2016	NVGRC	NVSS Giant Radio Sources Catalog
Gamma-ray	2016	MGRO	Milagro Gamma-Ray Observatory source list
Optical	2016- ...	Gaia DR(n)	*Gaia* Data Release (n) source
Gamma-ray	2017	2HWC	HAWC Observatory first catalog

AGN/radio galaxy. In some cases, the gamma-ray position may relate to the radio emission of the jet or lobe of an AGN, while the name refers to the radio core, which could be offset by a few arcseconds. This is manifest in the two different gamma-ray point-source components of Cen A (designed as Cen A core and Cen A lobe in the 4FGL). Another example is 4FGL J1758.7−1621 associated with AT20G J175841−161703 (also known as NVSS J175841−161705). This steep-spectrum AT20G radio source has a brighter neighbor (23.9 Jy at 160 MHz), PMN J1758−1616 (not included in the 3C catalog, because it lies 4° off the Galactic plane) at about 10″ offset. The radio structure map reveals that PMN J1758−1616 is an FR-II radio galaxy, while AT20G J175841−161703 corresponds to its radio lobe.

ORCID iDs

M. Axelsson https://orcid.org/0000-0003-4378-8785
J. Ballet https://orcid.org/0000-0002-8784-2977
G. Barbiellini https://orcid.org/0000-0003-1720-9727
D. Bastieri https://orcid.org/0000-0002-6954-8862
J. Becerra Gonzalez https://orcid.org/0000-0002-6729-9022
R. Bellazzini https://orcid.org/0000-0002-2469-7063
E. Bissaldi https://orcid.org/0000-0001-9935-8106
F. Cafardo https://orcid.org/0000-0002-7910-2282
C. C. Cheung https://orcid.org/0000-0002-4377-0174
F. D'Ammando https://orcid.org/0000-0001-7618-7527
R. de Menezes https://orcid.org/0000-0001-5489-4925
A. Desai https://orcid.org/0000-0001-7405-9994
A. Domínguez https://orcid.org/0000-0002-3433-4610
J. Finke https://orcid.org/0000-0001-5941-7933
A. Franckowiak https://orcid.org/0000-0002-5605-2219
Y. Fukazawa https://orcid.org/0000-0002-0921-8837
S. Funk https://orcid.org/0000-0002-2012-0080
P. Fusco https://orcid.org/0000-0002-9383-2425
F. Gargano https://orcid.org/0000-0002-5055-6395
S. Garrappa https://orcid.org/0000-0003-2403-4582
D. Gasparrini https://orcid.org/0000-0002-5064-9495
M. Giroletti https://orcid.org/0000-0002-8657-8852
S. Guiriec https://orcid.org/0000-0001-5780-8770
F. Krauss https://orcid.org/0000-0001-6191-1244
M. Kuss https://orcid.org/0000-0003-1212-9998
S. Larsson https://orcid.org/0000-0003-0716-107X
J. Li https://orcid.org/0000-0003-1720-9727
I. Liodakis https://orcid.org/0000-0001-9200-4006
F. Longo https://orcid.org/0000-0003-2501-2270
F. Loparco https://orcid.org/0000-0002-1173-5673
B. Lott https://orcid.org/0000-0003-2186-9242
P. Lubrano https://orcid.org/0000-0003-0221-4806
S. Maldera https://orcid.org/0000-0002-0698-4421
A. Manfreda https://orcid.org/0000-0002-0998-4953
F. Massaro https://orcid.org/0000-0002-1704-9850
M. N. Mazziotta https://orcid.org/0000-0001-9325-4672
N. Mirabal https://orcid.org/0000-0002-7021-5838
T. Mizuno https://orcid.org/0000-0001-7263-0296
M. E. Monzani https://orcid.org/0000-0002-8254-5308
A. Morselli https://orcid.org/0000-0002-7704-9553
I. V. Moskalenko https://orcid.org/0000-0001-6141-458X
R. Nemmen https://orcid.org/0000-0003-3956-0331
V. S. Paliya https://orcid.org/0000-0001-7774-5308
M. Pesce-Rollins https://orcid.org/0000-0003-1790-8018
S. Rainò https://orcid.org/0000-0002-9181-0345
M. Razzano https://orcid.org/0000-0003-4825-1629
O. Reimer https://orcid.org/0000-0001-6953-1385
F. K. Schinzel https://orcid.org/0000-0001-6672-128X
C. Sgrò https://orcid.org/0000-0001-5676-6214
D. J. Thompson https://orcid.org/0000-0001-5217-9135

References

Aartsen, M. G., Abraham, K., Ackermann, M., et al. 2017, ApJ, 835, 45
Abdo, A. A., Ackermann, M., Agudo, I., et al. 2010a, ApJ, 716, 30
Abdo, A. A., Ackermann, M., Ajello, M., et al. 2010b, ApJS, 188, 405, (1FGL)
Abdo, A. A., Ackermann, M., Ajello, M., et al. 2010c, ApJ, 720, 912
Abdollahi, S., Ackermann, M., Ajello, M., et al. 2017, ApJ, 846, 34
Abdollahi, S., Ackermann, M., Ajello, M., et al. 2018, Sci, 362, 1031
Acero, F., Ackermann, M., Ajello, M., et al. 2015, ApJS, 218, 23
Ackermann, M., Ajello, M., Allafort, A., et al. 2011, ApJ, 743, 171
Ackermann, M., Ajello, M., Atwood, W. B., et al. 2015, ApJ, 810, 14
Ackermann, M., Ajello, M., Baldini, L., et al. 2016, ApJ, 826, 1
Ackermann, M., Ajello, M., Baldini, L., et al. 2017, ApJL, 837, L5
Ackermann, M., Ajello, M., Baldini, L., et al. 2018, ApJS, 237, 32

Ahn, C. P., Alexandroff, R., Allende Prieto, C., et al. 2012, ApJS, 203, 21
Ajello, M., Shaw, M. S., Romani, R. W., et al. 2012, ApJ, 751, 108
Aldcroft, T. L., Siemiginowska, A., Elvis, M., et al. 2003, ApJ, 597, 751
Aleksić, J., Ansoldi, S., Antonelli, L. A., et al. 2015, A&A, 576, A126
Álvarez Crespo, N., Masetti, N., Ricci, F., et al. 2016a, AJ, 151, 32
Álvarez Crespo, N., Massaro, F., D'Abrusco, R., et al. 2016b, Ap&SS, 361, 316
Álvarez Crespo, N., Massaro, F., Milisavljevic, D., et al. 2016c, AJ, 151, 95
Angelakis, E., Hovatta, T., Blinov, D., et al. 2016, MNRAS, 463, 3365
Arsioli, B., & Chang, Y. L. 2017, A&A, 598, A134
Arsioli, B., & Polenta, G. 2018, A&A, 616, A20
Berton, M., Foschini, L., Ciroi, S., et al. 2015, A&A, 578, A28
Böck, M., Kadler, M., Müller, C., et al. 2016, A&A, 590, A40
Boller, T., Freyberg, M. J., Trümper, J., et al. 2016, A&A, 588, A103
Böttcher, M. 2007, Ap&SS, 309, 95
Broderick, A. E., Tiede, P., Chang, P., et al. 2018, ApJ, 868, 87
Bruel, P., Burnett, T. H., Digel, S. W., et al. 2018, arXiv:1810.11394
Caccianiga, A., Marchã, M. J., Antón, S., Mack, K., & Neeser, M. J. 2002, MNRAS, 329, 877
Capetti, A., Massaro, F., & Baldi, R. D. 2017a, A&A, 598, A49
Capetti, A., Massaro, F., & Baldi, R. D. 2017b, A&A, 601, A81
Capetti, A., & Raiteri, C. M. 2015, A&A, 580, A73
Cash, W. 1979, ApJ, 228, 939
Chang, Y.-L., Arsioli, B., Giommi, P., & Padovani, P. 2017, A&A, 598, A17
Chiaro, G., Salvetti, D., La Mura, G., et al. 2016, MNRAS, 462, 3180
Ciprini, S. & Fermi-LAT Collaboration 2012, in AIP Conf. Ser. 1505, 5th International Meeting on High Energy Gamma-Ray Astronomy, ed. F. A. Aharonian, W. Hofmann, & F. M. Rieger (Melville, NY: AIP), 697
Condon, J. J., Cotton, W. D., Greisen, E. W., et al. 1998, AJ, 115, 1693
D'Abrusco, R., Massaro, F., Paggi, A., et al. 2014, ApJS, 215, 14
D'Ammando, F., Orienti, M., Larsson, J., & Giroletti, M. 2015a, MNRAS, 452, 520
D'Ammando, F., Orienti, M., Tavecchio, F., et al. 2015b, MNRAS, 450, 3975
de Menezes, R., Peña-Herazo, H. A., Marchesini, E. J., et al. 2019, A&A, 630, A55
de Ruiter, H. R., Arp, H. C., & Willis, A. G. 1977, A&AS, 28, 211
Dermer, C. D., Yan, D., Zhang, L., Finke, J. D., & Lott, B. 2015, ApJ, 809, 174
Di Mauro, M., Manconi, S., Zechlin, H.-S., et al. 2018, ApJ, 856, 106
Domínguez, A., Primack, J. R., Rosario, D. J., et al. 2011, MNRAS, 410, 2556
Fan, X.-L., & Wu, Q. 2018, ApJ, 869, 133
Finke, J. D., Razzaque, S., & Dermer, C. D. 2010, ApJ, 712, 238
Fornasa, M., Cuoco, A., Zavala, J., et al. 2016, PhRvD, 94, 123005
Fuhrmann, L., Angelakis, E., Zensus, J. A., et al. 2016, A&A, 596, A45
Garrappa, S., Buson, S., Franckowiak, A., et al. 2019, ApJ, 880, 103
Ghisellini, G., Righi, C., Costamante, L., & Tavecchio, F. 2017, MNRAS, 469, 255
Gilmore, R. C., Somerville, R. S., Primack, J. R., & Dominguez, A. 2012, MNRAS, 422, 3189
Goodrich, R. W. 1989, ApJ, 342, 224
Griffith, M. R., & Wright, A. E. 1993, AJ, 105, 1666
Hayashida, M., Stawarz, Ł., Cheung, C. C., et al. 2013, ApJ, 779, 131
Healey, S. E., Fuhrmann, L., Taylor, G. B., Romani, R. W., & Readhead, A. C. S. 2009, AJ, 138, 1032
Healey, S. E., Romani, R. W., Cotter, G., et al. 2008, ApJS, 175, 97
Healey, S. E., Romani, R. W., Taylor, G. B., et al. 2007, ApJS, 171, 61
Hernández-García, L., Panessa, F., Giroletti, M., et al. 2017, A&A, 603, A131
Itoh, R., Nalewajko, K., Fukazawa, Y., et al. 2016, ApJ, 833, 77
Jones, D. H., Read, M. A., Saunders, W., et al. 2009, MNRAS, 399, 683
Kagaya, M., Katagiri, H., Yoshida, T., & Fukuda, A. 2017, ApJ, 850, 33
Kanekar, N., & Chengalur, J. N. 2003, A&A, 399, 857
Kuźmicz, A., Jamrozy, M., Bronarska, K., Janda-Boczar, K., & Saikia, D. J. 2018, ApJS, 238, 9
Landoni, M., Massaro, F., Paggi, A., et al. 2015, AJ, 149, 163
Landoni, M., Paiano, S., Falomo, R., Scarpa, R., & Treves, A. 2018, ApJ, 861, 130
Lico, R., Giroletti, M., Orienti, M., et al. 2017, A&A, 606, A138
Lister, M. L., Aller, M., Aller, H., et al. 2011, ApJ, 742, 27
Lister, M. L., Homan, D. C., Hovatta, T., et al. 2019, ApJ, 874, 43
Lonsdale, C., Conrow, T., Evans, T., et al. 1998, in IAU Symp. 179, New Horizons from Multi-Wavelength Sky Surveys, ed. B. J. McLean et al. (Dordrecht: Kluwer), 450
Marchesi, S., Kaur, A., & Ajello, M. 2018, AJ, 156, 212
Marchesini, E. J., Peña-Herazo, H. A., Álvarez Crespo, N., et al. 2019, Ap&SS, 364, 5
Masci, F. J., Condon, J. J., Barlow, T. A., et al. 2001, PASP, 113, 10
Massaro, E., Maselli, A., Leto, C., et al. 2015, Ap&SS, 357, 75
Massaro, F., D'Abrusco, R., Landoni, M., et al. 2015a, ApJS, 217, 2
Massaro, F., Landoni, M., D'Abrusco, R., et al. 2015b, A&A, 575, A124
Massaro, F., Marchesini, E. J., D'Abrusco, R., et al. 2017, ApJ, 834, 113
Massaro, F., Masetti, N., D'Abrusco, R., Paggi, A., & Funk, S. 2014, AJ, 148, 66
Massaro, F., Thompson, D. J., & Ferrara, E. C. 2015c, A&ARv, 24, 2
Mattox, J. R., Wagner, S. J., Malkan, M., et al. 1997, ApJ, 476, 692
Mauch, T., Murphy, T., Buttery, H. J., et al. 2003, MNRAS, 342, 1117
Migliori, G., Siemiginowska, A., Sobolewska, M., et al. 2016, ApJL, 821, L31
Murphy, T., Sadler, E. M., Ekers, R. D., et al. 2010, MNRAS, 402, 2403
Nalewajko, K., & Gupta, M. 2017, A&A, 606, A44
Osterbrock, D. E., & Pogge, R. W. 1985, ApJ, 297, 166
Padovani, P. 2007, Ap&SS, 309, 63
Padovani, P., Resconi, E., Giommi, P., Arsioli, B., & Chang, Y. L. 2016, MNRAS, 457, 3582
Paggi, A., Milisavljevic, D., Masetti, N., et al. 2014, AJ, 147, 112
Paiano, S., Falomo, R., Franceschini, A., Treves, A., & Scarpa, R. 2017a, ApJ, 851, 135
Paiano, S., Falomo, R., Treves, A., Franceschini, A., & Scarpa, R. 2019, ApJ, 871, 162
Paiano, S., Landoni, M., Falomo, R., et al. 2017b, ApJ, 837, 144
Paiano, S., Landoni, M., Falomo, R., Treves, A., & Scarpa, R. 2017c, ApJ, 844, 120
Paliya, V. S., Ajello, M., Rakshit, S., et al. 2018, ApJL, 853, L2
Paliya, V. S., Marcotulli, L., Ajello, M., et al. 2017, ApJ, 851, 33
Paragi, Z., Frey, S., Fejes, I., et al. 2000, PASJ, 52, 983
Peña-Herazo, H. A., Marchesini, E. J., Álvarez Crespo, N., et al. 2017, Ap&SS, 362, 228
Petrov, L., de Witt, A., Sadler, E. M., Phillips, C., & Horiuchi, S. 2019, MNRAS, 485, 88
Petrov, L., Mahony, E. K., Edwards, P. G., et al. 2013, MNRAS, 432, 1294
Planck Collaboration, Ade, N., Aghanim, P. A. R., et al. 2014, A&A, 571, A16
Pogge, R. W. 2000, NewAR, 44, 381
Prestage, R. M., & Peacock, J. A. 1983, MNRAS, 204, 355
Principe, G., Migliori, G., Johnson, T. J., et al. 2019, A&A, in press
Rakshit, S., Stalin, C. S., Chand, H., & Zhang, X.-G. 2017, ApJS, 229, 39
Ricci, F., Massaro, F., Landoni, M., et al. 2015, AJ, 149, 160
Ruan, J. J., Anderson, S. F., Plotkin, R. M., et al. 2014, ApJ, 797, 19
Schinzel, F. K., Petrov, L., Taylor, G. B., et al. 2015, ApJS, 217, 4
Schinzel, F. K., Petrov, L., Taylor, G. B., & Edwards, P. G. 2017, ApJ, 838, 139
Shaw, M. S., Filippenko, A. V., Romani, R. W., Cenko, S. B., & Li, W. 2013a, AJ, 146, 127
Shaw, M. S., Romani, R. W., Cotter, G., et al. 2013b, ApJ, 764, 135
Shen, Z.-Q., Jiang, D. R., Kameno, S., & Chen, Y. J. 2001, A&A, 370, 65
Sutherland, W., & Saunders, W. 1992, MNRAS, 259, 413
Tanaka, Y. T., Doi, A., Inoue, Y., et al. 2015, ApJL, 799, L18
Taylor, G. B., Wrobel, J. M., & Vermeulen, R. C. 1998, ApJ, 498, 619
The Fermi-LAT collaboration 2020, ApJS, 247, 33
Thompson, D. J., Ciprini, S., & Gasparrini, D. 2015, AAS Meeting, 225, 144.41
Tingay, S. J., & de Kool, M. 2003, AJ, 126, 723
Véron-Cetty, M.-P., & Véron, P. 2010, A&A, 518, A10
Voges, W., Aschenbach, B., Boller, T., et al. 1999, A&A, 349, 389
Voges, W., Aschenbach, B., Boller, T., et al. 2000, yCat, 9029, 0
Zargaryan, D., Sahakyan, N., & Harutyunian, H. 2018, IJMPD, 27, 1844022